

RESEARCH ARTICLE

10.1029/2020JD033219

Key Points:

- Biomass burning from peninsula Southeast Asia dominates the black carbon column burden in biomass burning sector (80%) over South China
- BC outflow/inflow from North China dominates the BC decrease/increase over South China induced by early/late East Asian summer monsoon onset
- Variation in East Asian summer monsoon onset times dominates the interannual variation of BC over South China in spring

Supporting Information:

- Supporting Information S1

Correspondence to:

B. Zhu and C. Pan,
binzhu@nuist.edu.cn;
arthur_pc@163.com

Citation:

Fang, C., Zhu, B., Pan, C., Yun, X., Ding, D., & Tao, S. (2020). Regional and sectoral sources for black carbon over South China in spring and their sensitivity to East Asian summer monsoon onset. *Journal of Geophysical Research: Atmospheres*, 125, e2020JD033219. <https://doi.org/10.1029/2020JD033219>

Received 9 JUN 2020

Accepted 8 SEP 2020

Accepted article online 30 SEP 2020

Author Contributions:

Conceptualization: Chenwei Fang,

Bin Zhu

Data curation: Chenwei Fang**Formal analysis:** Chenwei Fang**Funding acquisition:** Bin Zhu**Investigation:** Chenwei Fang**Methodology:** Chenwei Fang,

Chen Pan

Project administration: Bin Zhu,

Deping Ding

Resources: Bin Zhu, Xiao Yun,

Shu Tao

Software: Chenwei Fang, Chen Pan**Supervision:** Bin Zhu, Shu Tao**Validation:** Chenwei Fang, Bin Zhu**Visualization:** Chenwei Fang

(continued)

Regional and Sectoral Sources for Black Carbon Over South China in Spring and Their Sensitivity to East Asian Summer Monsoon Onset

Chenwei Fang^{1,2,3,4} , Bin Zhu^{1,2,3,4} , Chen Pan^{5,6}, Xiao Yun⁷, Deping Ding^{8,9}, and Shu Tao⁷ 

¹Collaborative Innovation Centre on Forecast and Evaluation of Meteorological Disasters, Nanjing University of Information Science and Technology, Nanjing, China, ²Key Laboratory for Aerosol-Cloud-Precipitation of China Meteorological Administration, Nanjing University of Information Science and Technology, Nanjing, China, ³Key Laboratory of Meteorological Disaster, Ministry of Education (KLME), Nanjing University of Information Science and Technology, Nanjing, China, ⁴Special test field of National Integrated meteorological observation, Nanjing University of Information Science and Technology, Nanjing, China, ⁵Jiangsu Meteorological Observatory, Nanjing, China, ⁶Key Laboratory of Transportation Meteorology, China Meteorological Administration, Nanjing, China, ⁷Laboratory for Earth Surface Processes, College of Urban and Environmental Sciences, Peking University, Beijing, China, ⁸Beijing Weather Modification Office, Beijing, China, ⁹Beijing Key Laboratory of Cloud, Precipitation and Atmospheric Water Resources, Beijing, China

Abstract Besides local emissions, biomass burning (BB) emissions in peninsula Southeast Asia (PSEA) and domestic anthropogenic emissions in North China (NC) are also significant black carbon (BC) sources over South China (SC) in spring. Meanwhile, the East Asian summer monsoon (EASM) is established with the wind field reversal, influencing the region-based contributions to BC over SC. Herein, BC sources for SC were tracked by region and by sector using the Community Earth System Model with a BC-tagging technique. During the spring of 2000–2014, 27% of BC surface concentration (BCS) and 64% of BC column burden (BCC) over SC stems from nonlocal sources. BC from NC is mainly transported below 850 hPa. It is the dominant nonlocal contribution to BCS (17%) and largely composed of residential and industrial sectors. Nonlocal emissions inside and outside China contribute 28% and 36% to BCC, respectively. Generally transported above 850 hPa, BC from PSEA is the largest nonlocal contributor (20%) to BCC and contributes 80% of BCC in BB sector. Additionally, the interannual variation in EASM onset times bring a maximum of -5% to $+7\%$ / -2% to $+7\%$ variation in BCC/BCS. The BC outflow/inflow contributed from NC dominates the BC decrease/increase over SC with southerly/northerly wind anomaly induced by early/late EASM onset, yet regional transport from PSEA contributes minor BC changes. The simulated BC is significantly positively correlated with the varying EASM onset times, but not with emissions, indicating the decisive role of meteorology in the interannual variation of BC over SC during springtime.

1. Introduction

Black carbon (BC) is mainly emitted from the incomplete combustion of fossil fuels, biofuels, and biomass burning (Bond et al., 2004). BC can induce significant environmental and climate effects as one of the main components of atmospheric fine particulate matter ($PM_{2.5}$) and absorbing aerosols (Menon et al., 2002). In addition to absorbing solar radiation, BC can serve as cloud condensation nuclei by mixing with hygroscopic aerosols, causing direct and indirect climate forcing on the Earth-atmosphere system (Jacobson, 2002; Ramaswamy et al., 2001; Twomey, 2007). Bond et al. (2013) revealed that the warming efficiency of BC is much higher than that of CO_2 and other greenhouse gases (GHGs) with the same mass. Moreover, recent studies have found that the heating effect of BC can inhibit the upward development of the boundary layer, increase the frequency of heavy haze events, and affect the surface ozone concentration in China, indicating that the radiative effects of BC may further aggravate environmental problems (Ding et al., 2016; Gao et al., 2018). Hence, the identification of BC sources is needed to help the government manage and reduce BC emissions in a targeted and strategic way.

Asia, especially China, serves as the major contributor to the BC concentration and radiative forcing (RF) worldwide because of its dense population and rapid acceleration in economic development

Writing - original draft:

Chenwei Fang

Writing - review & editing:

Chenwei Fang, Bin Zhu, Chen Pan,
Shu Tao

(Li, Gasser, et al., 2016; Qin & Xie, 2012). Although China has witnessed a decrease in BC emissions since the mid-1990s due to technological advances and energy reforms, BC emissions and concentrations are still relatively high (Wang et al., 2012). In addition, BC emissions from the developing countries close to China are continuously growing (Bond et al., 2013; Sahu et al., 2008). As a result, the BC sources in China and its surrounding regions have a complex composition. Located in the southern part of China, South China (SC) is the fastest-growing economic area and one of the most developed regions in China (Zhong et al., 2013). Urbanization and economic development in this region cause air pollution and frequent haze events (Kwok et al., 2010; Wang, Lyu, et al., 2016). Lan et al. (2013) found that BC accounted for approximately 11% of the mass concentration of PM_{2.5} in SC via observations in megacities. Wu et al. (2013) obtained an average BC concentration of 12.3 μg m⁻³ at urban sites across SC from December 2008 to January 2009.

SC is located downwind of peninsula Southeast Asia (PSEA) in spring atmospheric circulation (Zhu et al., 2011). Previous studies have indicated that the high biomass burning (BB) emissions in PSEA during springtime have notable impacts on SC, Hong Kong, and even the Pacific region (Bey et al., 2001) and the Yangtze River Delta (Fu et al., 2012). Previous observational studies found that the aerosols transported into these regions contain a large amount of BC (Deng et al., 2008; Lin et al., 2013). Using the Community Multiscale Air Quality Modeling System (CMAQ) model, Huang et al. (2013) found that the high BB emissions from PSEA in March-April-May (MAM) contributed 26–62% of the aerosol optical depth (AOD) in its downwind regions (including SC, South China Sea, and Taiwan Strait). Zhang et al. (2014) reported that the high BC concentrations observed in Hainan, South China, corresponded to the times when high BB emission in PSEA occurred through in situ measurements and backward trajectory analysis. Besides, severe aerosol pollutions over North China (NC) have been widely reported (Fu et al., 2014). The domestic contribution from anthropogenic emission sectors in NC can also be a threat to the air quality over SC. Yang et al. (2017) found that 35% of the surface BC over SC in winter comes from NC through model simulation. However, spring haze pollution in NC are also frequently observed, and increased aerosol concentration has been detected during spring in recent years (Chen et al., 2018; Chen & Wang, 2015). Some observational and modeling studies have analyzed the BC sources over SC in spring but focused on individual sites or episodes (Deng et al., 2008; Tao et al., 2017; Wang, Huang, et al., 2016; Zhang et al., 2014; Zhang, Li, et al., 2010). These studies had no focus on the long-term region and sector source contributions to BC over SC in MAM.

Moreover, as one of the most influential monsoon systems in the world, the East Asian summer monsoon (EASM, including the East Asian subtropical summer monsoon and the South China Sea tropical summer monsoon) is established and the wind direction starts to reverse over SC in MAM due to the reversal of the land-sea thermal contrast between the Asian continent and the western Pacific (He et al., 2008; Zhu et al., 1986, 2011). The monsoon has decisive effects on the distribution, transport, and deposition of aerosols (Guo et al., 2014; Niu et al., 2010; Wu et al., 2016). However, most studies have focused on how the changes in EASM and the East Asian winter monsoon (EAWM) strengths (represented as the EASM/EAWM index) impact aerosols in summer and winter (Li, Zhang, & Wang, 2016; Mao et al., 2017; Yang et al., 2014; Zhang, Liao, & Li, 2010; Zhu et al., 2012). Some studies have investigated the relationship between the monsoon onset and aerosols and found that anthropogenic aerosols may lead to the advance in the monsoon onset time in MAM (Bollasina et al., 2013; Wang, Zhu, et al., 2016), whereas the variations in aerosol distributions and sources caused by the interannual variation in monsoon onset times remain unclear. SC is under the control of East Asian subtropical summer monsoon during the summer half-year (Li & Zeng, 2003; Wang & Lin, 2002). Unlike the tropical monsoon transition when the lower zonal wind changes from winter easterlies to summer westerlies, the EASM over SC establishes the seasonal transition manifesting as the reversal of meridional wind direction in MAM (Luo & Lin, 2017; Wang & Lin, 2002). Lying at the front of the continental part of the EASM control region, the conversion from prevailing northerly wind to southerly wind caused by the seasonal shift of the continent-sea thermal condition is established first in March to April over SC and gradually moves northward (He et al., 2008; Qi et al., 2007; Zhu et al., 2011). Thus, the source region contributions to BC over SC in MAM will be influenced due to the wind field reversal.

The emission sensitivity approach and BC-tagging technique applied in the model are two widely used methods to analyze BC sources in large areas for long periods (Li, Liao, et al., 2016; Wang, Rasch, Easter, et al., 2014; Zhang, Wang, Hegg, et al., 2015; Zhang, Wang, Qian, et al., 2015; Zhuang et al., 2019). Compared with the former method, which requires multiple emission perturbation simulations, the BC-tagging technique

generates more computational and accurate results when identifying BC sources (Wang, Rasch, Easter, et al., 2014). The source-receptor relationships for BC in various countries and regions (e.g., the United States, China, Arctic, Himalayas and Tibetan Plateau, TP) have been investigated with this method (Wang, Rasch, Easter, et al., 2014; Yang et al., 2017, 2018; Zhang, Wang, Hegg, et al., 2015; Zhang, Wang, Qian, et al., 2015). This method has also been used to track the BC sources in the production and consumption perspective (Meng et al., 2018). For the sector contributions, Li, Liao, et al. (2016) quantified the contributions from residential (Res), industry (Ind), transportation (Tra), energy (Ene), and BB to BC in China, but their simulations were based on the emission sensitivity approach.

Here, a BC-tagging technique was applied to the Community Earth System Model (CESM) to enable simultaneous tracking of the region and sector sources of BC over SC. The primary scope of this study is to distinguish the relative contributions of local emissions and regional transport from various regions inside and outside China to the BC concentration over SC in MAM. The long-term contribution of BB emissions from PSEA also needs to be identified. Moreover, with the control experiment and an experiment isolating the disturbance of meteorological factors by fixing BC emissions, the impacts of the variation in EASM onset times on the interannual variations in BC concentrations and sources over SC were studied. Descriptions about the model, BC inventories and BC-tagging method are provided in section 2. Model evaluations and analysis of the region and sector source contributions to BC over SC during springtime are presented in sections 3.1–3.4. Section 3.5 clarifies the impacts of the interannual variation in EASM onset times on BC in MAM. Uncertainties in the simulated results are discussed in section 3.6. Conclusions are given in section 4.

2. Data and Methods

2.1. Model Description, Configuration, and BC Emissions

BC sources were simulated and tracked based on CESM Version 1.0.4 (Hurrell et al., 2013) with its atmospheric component CAM5 (Community Atmosphere Model Version 5; Neale et al., 2012). Simulations were conducted with a horizontal resolution of $1.9^\circ \times 2.5^\circ$ and 56 vertical levels from the surface to 4 hPa, using prescribed climatological sea surface temperatures and sea ice distribution. The model specifies the lower boundary condition and advects the GHGs (CH_4 , H_2 , N_2O , etc.) in the atmosphere. CO_2 is assumed to be well mixed with a time invariant surface value. The model uses the deep convection scheme from Zhang and McFarlane (1995) with modifications (e.g., Richter & Rasch, 2008) and shallow convection scheme from Park and Bretherton (2009). Vertical diffusion in the boundary layer was illustrated by Holtslag and Boville (1993). The resistance approach in Wesely (1989) is adopted for the dry deposition scheme with several updates (e.g., Wesely & Hicks, 2000). The wet removal scheme is parameterized from Horowitz et al. (2003). Aerosols including BC, sulfate, primary and secondary organic compounds, ammonium nitrate, and sea salt are calculated based on the MOZART-4 chemical mechanism (Emmons et al., 2010). A lognormal distribution is assumed for aerosols except for sea salt with the bulk aerosol model (Lamarque et al., 2012). BC is emitted in hydrophobic and hydrophilic forms (80% and 20%, respectively) with a fixed aging timescale of 1.6 days (Cooke & Wilson, 1996). The two forms are considered to be mixed externally with respect to each other, but BC in hydrophilic form is internally mixed, which can activate cloud droplets (Emmons et al., 2010; Sadiq et al., 2015; Stevens & Dastoor, 2019). The dynamic parameterization scheme adopted is the finite volume dynamical core, with emphasis on the conservation, accuracy, and efficiency of the tracer transport process (Rasch et al., 2006). In this study, the meteorology fields (e.g., horizontal winds, air and surface temperature, surface pressure, heat fluxes, and wind stresses) were nudged to Modern Era Retrospective analysis for Research and Applications (MERRA) data sets (Rienecker et al., 2011) with a time resolution of 6 hours. All fields are linearly interpolated to avoid jumps for time steps between the reading times (Lamarque et al., 2012). CAM5 uses a substepping procedure (Lauritzen et al., 2011) and an atmospheric mass fixer algorithm (Rotman et al., 2004) to ensure consistency between the inserted and model-computed velocity and mass fields. Previous studies have compared aerosol properties (concentration, AOD, etc.) and meteorological fields (wind, temperature, precipitation, humidity, etc.) with various data sets and validated the performance of CESM with such configurations (Pan et al., 2017; Tosca et al., 2013; Zhang, Wang, Hegg, et al., 2015).

The Peking University BC inventory (PKU-BC; Wang, Tao, Shen, et al., 2014) was used for anthropogenic BC emissions. PKU-BC is a global monthly emission inventory covering the period of 1960 to 2014. This

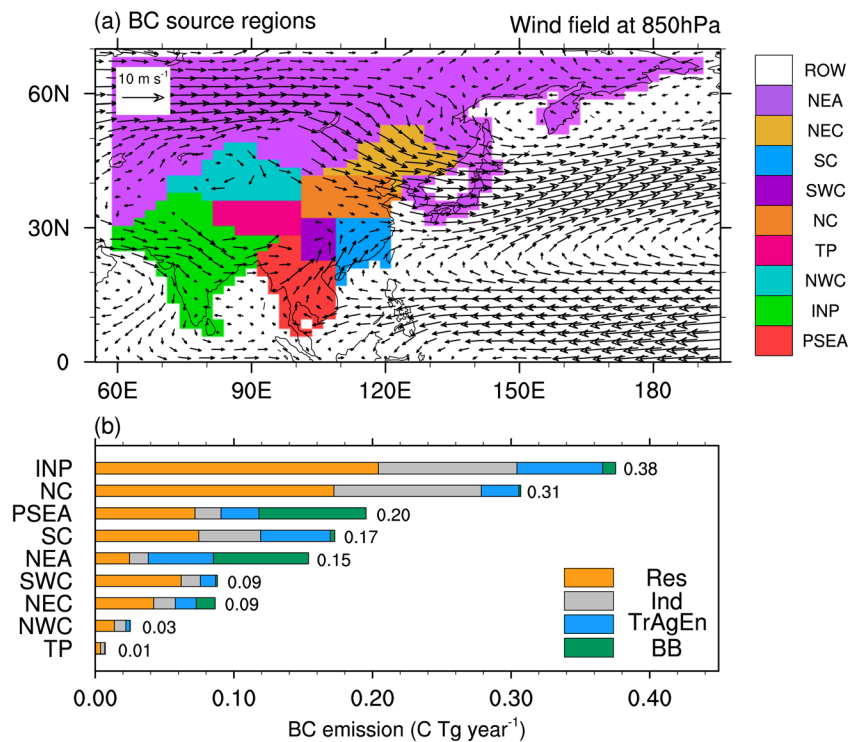


Figure 1. (a) Tagged source regions of black carbon (BC; South China, SC; North China, NC; Southwest China, SWC; Northeast China, NEC; Northwest China, NWC; Tibetan Plateau, TP; peninsula Southeast Asia, PSEA; Indian peninsula, INP; Northeast Asia, NEA; and the rest of the world, ROW) and simulated MAM mean wind field (units: m s^{-1} , vectors) at 850 hPa during 2000–2014. (b) March–April–May (MAM) mean BC emissions (units: C Tg year^{-1}) from different sectors in tagged source regions during 2000–2014 based on PKU-BC and GFED v4.1s inventories. The BC emissions in ROW are not shown.

inventory considers emissions from Ene, Ind, Res, Tra, and agriculture (Agr) sectors. Considering the randomness of BB emissions over time, the Global Fire Emissions Database Version 4.1 s (GFED v4.1s) was chosen to quantify the daily BB emissions of BC from 2003 to 2014 (Randerson et al., 2017). We use the global scalar field of the daily fraction from GFED v4.1s to redistribute monthly emissions into daily time steps. GFED v4.1s considers small fires and gives a better match with field studies compared with previous versions (Van Der Werf et al., 2017).

2.2. BC-Tagging Method and Numerical Experiments

Given the generally short lifetime of BC (Samset et al., 2014), SC and its surrounding areas were separated into 10 regional sources (Figure 1). The blue area (18°N to 31.26°N , 108.75°E to 121.25°E) in Figure 1a denotes the SC area defined in the model. NC, Southwest China (SWC), Northeast China (NEC), Northwest China (NWC), and TP are the source regions inside China. PSEA, the Indian peninsula (INP), Northeast Asia (NEA), and the rest of the world (ROW) are the non-China source regions that may influence SC. Figure S1 in the supporting information shows the proportions of seasonal emissions to annual emissions of different regions. The BC emission amounts in almost all regions are roughly the same in MAM, June–July–August (JJA), and September–October–November (SON), and the largest proportion occurs in December–January–February (DJF), except for PSEA and NEA. The BC emissions in these two regions are the highest in MAM compared to in other seasons. Res and Ind are the main BC emission sectors in Asia (Zhuang et al., 2019). The BC emissions from the other anthropogenic sectors, including Tra, Agr, and Ene, are much lower and attain their highest values in eastern China and northern India (Li, Liao, et al., 2016; Wang et al., 2012). For efficiency and comparability when quantifying sector sources, BC from the Tra, Agr, and Ene sectors were tracked as a whole (TrAgEn) in our simulation. The contributions of four emission sectors (Res, Ind, TrAgEn, and BB) were tracked in this study, among which TrAgEn stands for the merged Tra, Agr, and Ene sectors. Considering that BC in MOZART-4 contains the hydrophilic and hydrophobic

components, 80 passively tagged BC species (10 regions \times 4 sectors \times 2 BC components) were added in the model. The simulation with tagged BC generates more accurate results than emission sensitivity simulations, which must assume a linear BC response (Wang, Rasch, Easter, et al., 2014).

Based on the BC parameterization schemes in the model, the time evolution of the mass mixing ratios (MMRs) of BC emitted from a specific tagged source is expressed as

$$\begin{aligned} \frac{\partial q_{tg(i,j,k)}}{\partial t} = & \left(\frac{\partial q_{tg(i,j,k)}}{\partial t} \right)_{diff} + \left(\frac{\partial q_{tg(i,j,k)}}{\partial t} \right)_{adv} + \left(\frac{\partial q_{tg(i,j,k)}}{\partial t} \right)_{dp\ conv} + \left(\frac{\partial q_{tg(i,j,k)}}{\partial t} \right)_{shlw\ conv} \\ & + \left(\frac{\partial q_{tg(i,j,k)}}{\partial t} \right)_{chem} + \left(\frac{\partial q_{tg(i,j,k)}}{\partial t} \right)_{dry\ depo} + \left(\frac{\partial q_{tg(i,j,2)}}{\partial t} \right)_{wet\ depo} \end{aligned} \quad (1)$$

where $q_{tg(i,j,k)}$ represents the tracked BC MMRs assigned to region i ($i = 1, 2, \dots, 10$), sector j ($j = 1, 2, \dots, 4$), and component k ($k = 1$ and 2 for hydrophobic and hydrophilic BC, respectively). The terms on the right-hand side of Equation 1 denote the tendencies of tagged BC in various processes, including vertical diffusion (diff), advection (adv), deep convection (dp conv), shallow convection (shlw conv), chemistry (chem), dry deposition (dry depo), and wet deposition (wet depo). For the temporal evolution of $q_{tg(i,j,k)}$ in dry deposition, it is calculated in the same way as that of original BC, but the relevant variable of tagged BC is substituted for the corresponding variable of original BC, expressed as

$$\left(\frac{\partial q_{tg(i,j,k)}}{\partial t} \right)_{dry\ depo} = \frac{P_{surf}}{R_{air} T_{surf}} DV_k q_{tg(i,j,k)} \quad (2)$$

where P_{surf} is the midpoint pressure in surface layer, R_{air} is the dry air gas constant, T_{surf} is the temperature in surface layer, and DV_k is the deposition velocity of BC species. The ratio between the MMR of tagged hydrophilic BC ($k = 2$) and the corresponding sum is used to calculate the wet deposition tendency of tagged BC:

$$\left(\frac{\partial q_{tg(i,j,2)}}{\partial t} \right)_{wet\ depo} = \frac{q_{tg(i,j,2)}}{\sum_{\substack{1 \leq i \leq 10 \\ 1 \leq j \leq 4}} q_{tg(i,j,2)}} \left(\frac{\partial q}{\partial t} \right)_{wet\ depo} \quad (3)$$

where $\left(\frac{\partial q}{\partial t} \right)_{wet\ depo}$ is the wet deposition tendency of original BC. For the other processes, the temporal evolution of $q_{tg(i,j,k)}$ is treated with the same parameterization subroutines as the original BC. All tagged BC species are independent and passive, which means they have no impact on dynamical and thermal fields. The difference between the MMR of original BC and the summed MMRs of tagged BC is negligible compared with the BC concentration (Figure S2). This difference is caused by the nonlinearities in the calculations of the tendencies of BC in the physical schemes.

Two experiments were designed in this study. Experiment CTRL included the varying BC emissions and meteorological factors from 2000 to 2014. To elucidate the BC variation induced by meteorological factors, BC emissions were fixed at the averaged value between 2000 and 2014 in experiment n_vEMIS to examine how interannual variation in EASM onset times impacts BC. Meteorological factors were isolated and varied with time in n_vEMIS. As GFED v4.1s does not include daily emissions prior to 2003, the BB emissions for this period were based on the data of 2003. Region and sector sources of BC were tracked in both experiments. Experimental outputs were set to a pentad (5 days) average instead of the usual monthly resolution to confirm the EASM onset times.

3. Results

3.1. Model Evaluations

Figures 2a–2d show the spatial distributions of the BC surface concentration (BCS) and BC column burden (BCC) from the simulations and MERRA Version2 (MERRA2; Gelaro et al., 2017). The MERRA2 BC data in China have been verified and applied in previous studies (Sun et al., 2019, etc.) and this study

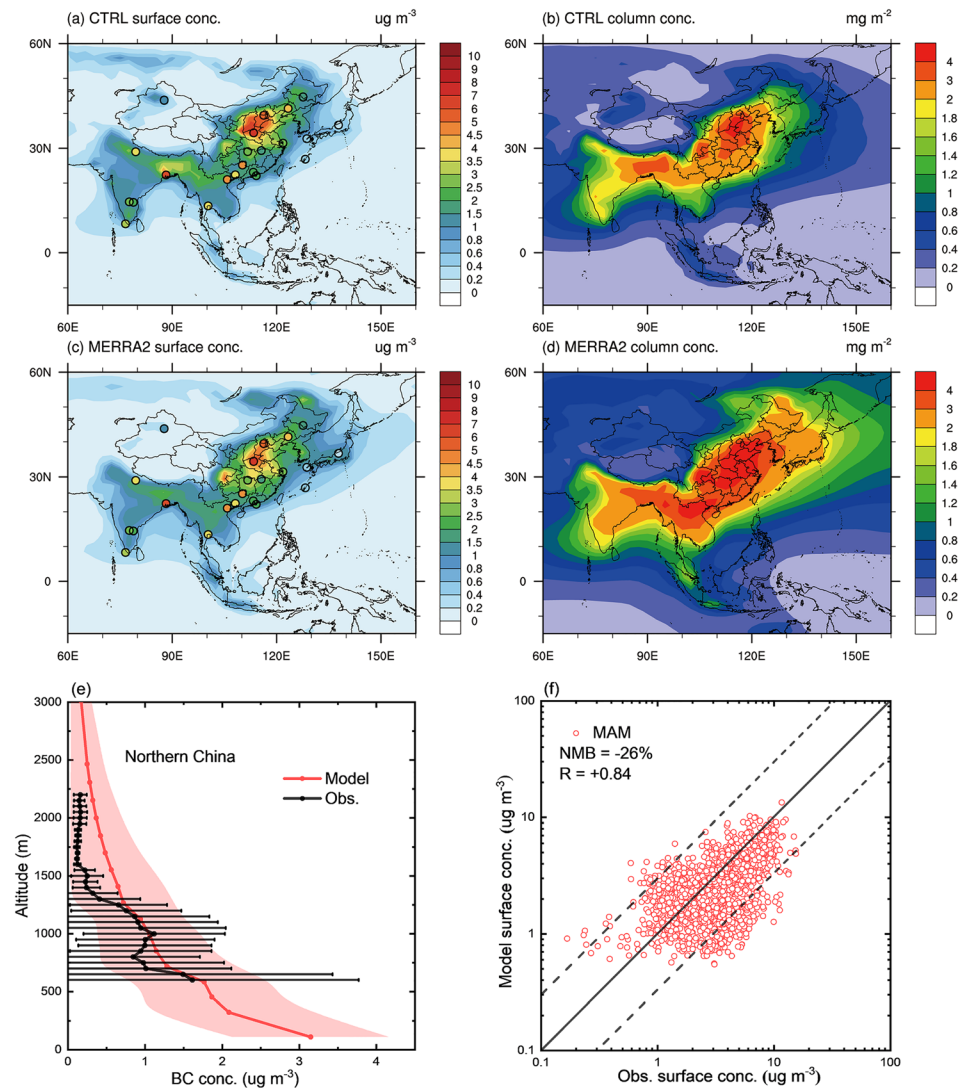


Figure 2. Spatial distributions of the MAM mean BC surface concentration (BCS; units: $\mu\text{g m}^{-3}$; a, c) and BC column burden (BCC; units: mg m^{-2} ; b, d) from the model results and MERRA2 data during 2000–2014 (the dots in a and c represent the observed BC concentrations at the different sites). (e) A comparison of the vertical distributions of the MAM mean BC concentration (units: $\mu\text{g m}^{-3}$) from the model results (dark red lines; the light red shading denotes the standard deviation) and observations (black lines; the thin horizontal error bars denote the standard deviation). (f) The scatterplot of the pentad mean BC concentration (units: $\mu\text{g m}^{-3}$) between the model results and observations in MAM (normalized mean bias (NMB; $\text{NMB} = 100\% \times \Sigma (M_i - O_i) / \Sigma O_i$, where i represents each site, M represents the simulation value, and O represents the observation value) and correlation coefficient (R) are shown in the top left corner. The dashed lines mark the 1:3 and 3:1 ratios. The solid line marks the 1:1 ratio).

(Figure S3). The observed BCS values are scattered in Figures 2a and 2c. The BCS data in China and at 10 other sites in PSEA, INP and NEA come from the China Meteorological Administration and previous studies (Babu & Moorthy, 2002; Begam et al., 2016; Cheng et al., 2006; Cohen et al., 2010; Joshi et al., 2016; Kalluri et al., 2017; Matsui et al., 2013; Sahu et al., 2011; Talukdar et al., 2015). The site locations and sampling periods are summarized in supporting information Table S1. The spatial distributions of BCS and BCC are reasonably reproduced. Notably, the model results can reproduce relatively high BCS values over certain small areas near Urumchi (China), Kolkata (India), and Pantnagar (India), but MERRA2 exhibits a small bias locally. The simulated BCC values are generally lower than those from MERRA2, especially in remote and sea areas with low BC emissions. The vertical distribution of simulated BC is verified against the observed

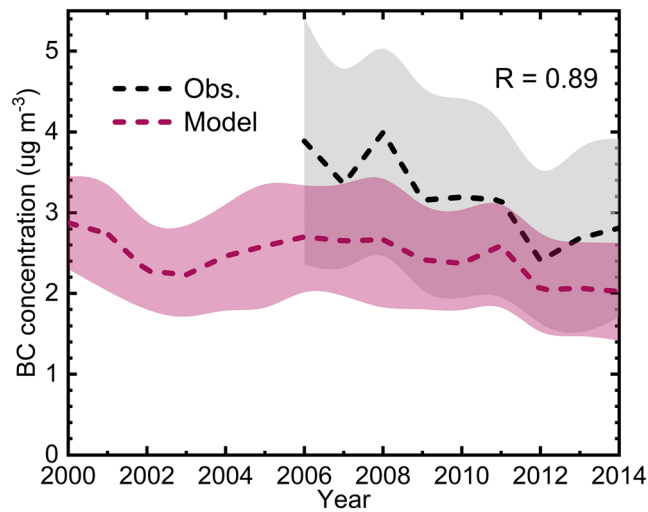


Figure 3. Interannual variations of MAM mean BC surface concentrations (units: $\mu\text{g m}^{-3}$) from observations (black dashed line) and model results (red dashed line) at six sites in SC. Light color shadings denote the standard deviations of simulated and observed BC. The correlation coefficient (R) between them calculated over the time period of 2006–2014 is shown at the top right corner.

BC from Zhao et al. (2015) (Figure 2e). Overall, the model results agree well with the observations and reflect the vertical variation characteristics of BC over NC.

The MAM mean BC surface concentrations in China are underestimated by -26% in the model (Figure 2f). The model biases in BC in the other seasons range from -34% to $+3\%$ (figure not shown). Figure S4 shows the other simulated BC results with the MIX Version 1.1 (Li et al., 2017) and REAS (Regional Emission inventory in Asia) Version 1.11 (Ohara et al., 2007) emission inventories. The biases in the simulated BC concentrations in China based on the PKU-BC inventory in all seasons are lower than those in the simulation results based on other inventories, especially in DJF. Wang, Tao, Balkanski, et al. (2014) explained the reason for the lower bias (-35%) in the simulated BC in Asia based on PKU-BC, which allows the per capita fuel consumption to vary across different regions with subnational fuel consumption data. Model also captures the interannual peaks and troughs of the observed MAM mean BCS over SC, with a high-correlation coefficient of 0.89 (Figure 3). The time series of the pentad mean BCS in China in MAM can be seen in Figure S5, and the correlation coefficients between the simulations and observations pass the significance test ($p < 0.01$).

3.2. Regional Sources

The spatial distributions of the absolute and relative contributions of regional sources to BCS and BCC over SC in MAM are shown in Figure 4. The average BCS concentration in SC is approximately $1.39 \mu\text{g m}^{-3}$ in MAM, 26.7% of which is contributed by nonlocal emissions. Domestic emissions in NC are the primary contributor of all nonlocal sources, supplying approximately $0.24 \mu\text{g m}^{-3}$ (17.3%) of the BC concentration at the surface along with the northwesterly wind (Figure 1). The other regions contribute little to BCS in SC. SWC and PSEA contribute approximately $0.03 \mu\text{g m}^{-3}$ each. NEC, INP, and ROW contribute approximately $0.02 \mu\text{g m}^{-3}$ each (figure not shown). Because NEA is far away from SC in Asia and NWC and TP are clean areas, the BC transported from these regions is negligible. The BC proportion from local emissions in SC decreases significantly from the surface to the upper air. A BCC proportion of 63.9% in the air over SC is imported from nonlocal sources, which indicates that the BCC over SC in MAM is mainly controlled by regional transport. Nonlocal emissions inside and outside China contribute 27.7% and 36.1% to BCC in SC, respectively. Although the contribution of NC to BCC has a similar proportion (18.3%) as that to BCS, the contributions of regional sources outside China surpass that of NC and are the main nonlocal source of BCC over SC. Transported by the strong southwesterly wind in MAM (Figure 1), BC emitted from PSEA accounts for 19.8% of the total BCC over SC, second to the impact of local emissions (36.1%). INP is the third largest nonlocal BCC source, accounting for 12.4% of the overall BCC. BC transport from the other nonlocal sources also increases from the surface to the upper air, with a joint contribution of 13.4% to the BCC. These results suggest the equal importance of the impacts of emissions from inside and outside China on BC over SC. In contrast to the surface BCS, where the main nonlocal sources are within China, the nonlocal BCC over SC is mainly provided by regions outside China.

Note that the BCC value over SC in MAM is close to that in DJF due to the large contributions of nonlocal sources; however, the local BC emission amounts in MAM are much smaller than that in DJF (Figure 5). Figure S6 shows that nonlocal source contributions to BC over SC are also significant in DJF and the domestic emission from NC is the main nonlocal source, which is consistent with the results from Yang et al. (2017).

3.3. Sectoral Sources

The contributions from the Res, Ind, TrAgEn and BB sectors to BC concentrations over SC range from large to small (Figure 6). Res is the primary emission sector of BCS and BCC over SC. Nearly half of BCS and BCC over SC can be attributed to Res from 2000 to 2014, with absolute (relative) contributions of $0.64 \mu\text{g m}^{-3}$

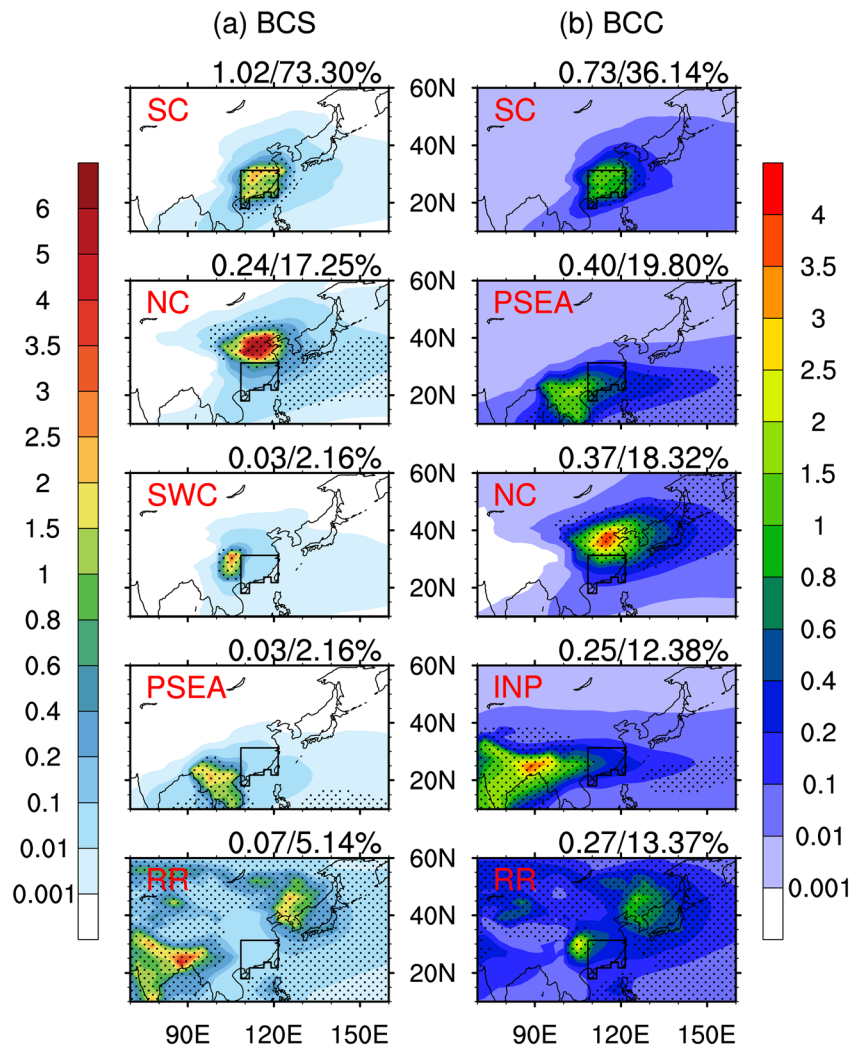


Figure 4. (a) Spatial distributions of the contributions (units: $\mu\text{g m}^{-3}$; shading) to MAM mean BCS from main regional sources and remaining regional (RR) sources. (b) Same as (a), but for the regional contributions (units: mg m^{-2} ; shading) to MAM mean BCC. The panels are ordered by the contributions to BC from main regional sources. The region enclosed by black lines represents SC. The averaged absolute and relative contributions of each regional source to BC over SC are given at the top right of the panel. The dotted areas indicate that the relative contribution (units: %) of the regional source exceeds 20%.

(46.0%) and 0.94 mg m^{-2} (46.5%) to BCS and BCC, respectively. According to section 3.2, local area, NC, and PSEA are the major source regions of BC over SC. With the help of the BC regional and sectoral source tracking method, Figure 7 shows the spatial distributions of the relative contributions from SC, NC and PSEA to BC over SC by the different sectors. Approximately 54.4% of BCS in the Res sector comes from local emissions, followed by BCS transported from NC (25.9%). The contributions of SC and NC emissions to BC in the Res sector decrease in the upper air with a joint contribution of 50% to BCC. Res is the main BC emission sector in Asia (accounting for 50% or more of BCS and BCC) in MAM except for some areas in PSEA and NEA.

The Ind sector is the second largest contributor to BC over SC, accounting for 25.9% ($0.36 \mu\text{g m}^{-3}$) of BCS and 22.3% (0.45 mg m^{-2}) of BCC. BC emitted from TrAgEn supplies 25.2% ($0.35 \mu\text{g m}^{-3}$) of BCS and 18.32% (0.37 mg m^{-2}) of BCC averaged over SC, which is slightly lower than the contribution from Ind (Figure 6). Similar to the characteristics of the regional sources of BC in the Res sector, 80–90% of the BCS from the Ind and TrAgEn sectors over SC is attributed to local and NC emissions, and emissions from

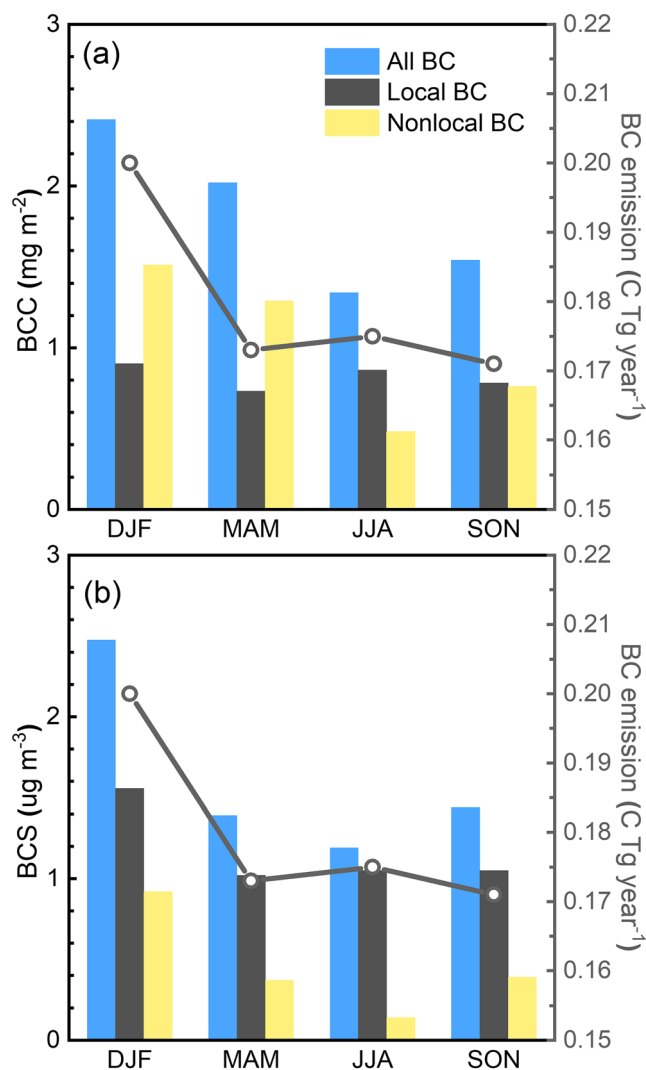


Figure 5. Seasonal variations in BC concentrations contributed by all (blue bars), local (black bars), and nonlocal (yellow bars) source regions over SC and the regional mean BC emissions (units: C Tg year⁻¹; lines) from PKU-BC and GFED v4.1s inventories during 2000–2014. (a) is for BCC (units: mg m⁻²) and (b) is for BCS (units: µg m⁻³).

these two regions have relatively small impacts on BCC in Ind and TrAgEn sectors (Figure 7). In addition, Figure 7b1 shows that little BCS and BCC in the TrAgEn sector (6.67%) and BB sector (1.74%) are contributed by NC, indicating that the BC transported from NC may be mainly attributed to the Res and Ind sectors. This will be examined in detail in section 3.4.

In contrast to the anthropogenic sectors, the highest values of BC originating from the BB sector occur over PSEA with BC concentrations exceeding 1.5 µg m⁻³ and 1.5 mg m⁻². Over SC, little BCS originates from the BB sector (0.04 µg m⁻³, 2.9%) due to the low local BB emissions (Figure 7a1). However, the contribution of the BB sector reaches 12.9% of BCC in the air (Figure 6b2), comparable with the joint contribution (18.3%) of the Tra, Agr, and Ene sectors. By analyzing the regional contributions to BC in the BB sector, Figure 7c2 reveals that the majority of BC in the BB sector over SC is generated from PSEA. The high BB emissions from PSEA account for nearly 80% of BCC in the BB sector over SC, which is 10.3% of the total BCC over SC. Our result is consistent with the result of Chan (2017) They estimated that the BB emissions from PSEA could contribute 11% of the total BC in the air over Hong Kong using the global chemical transport model GEOS-Chem. Emissions from PSEA also provide 38.4% of BCS in the BB sector (accounting for 1.1% of the total BCS) at the surface of SC, almost equal to the contribution from local emissions (41.1%, Figures 7a1 and 7c1), though the analysis above suggests that the surface BC mainly comes from local emissions and regional transport from NC.

3.4. Vertical Distribution Characteristics of BC From Different Sources

Considering the different contribution characteristics of regional and sectoral sources to BCS and BCC, determining the source contributions to BC at different altitudes is valuable. Figure 8a shows that the BC concentration decreases rapidly with altitude over SC, with a gradually decreasing contribution of local emissions, while the influence of regional transport increases. The contribution of nonlocal sources to the BC concentration over SC exceeds the local emission contribution from 850 hPa. At least 60% of the BC above 850 hPa comes from regional transport, while the proportion increases to 80% above 750 hPa, indicating that most of the BC at higher altitudes over SC is imported from nonlocal sources (Figure 8b).

Note that the main transport height of BC varies with the different nonlocal sources. Figure 8c shows that regional transport from most domestic region sources mainly occurs in the lower troposphere, led by the contribution of NC (below 850 hPa). BC from NC accounts for 50–75% of the nonlocal BC in this layer. However, the BC amount from NC decreases with altitude, and emissions from non-China regions begin to dominate the BC concentration over SC, especially the emissions from PSEA and INP. BC transport from PSEA and INP to SC mainly occurs in the free troposphere (above 850 hPa), accounting for 55–74% of the total BC from nonlocal sources in this layer. Figure S7 reveals that the height of the high-value center of BC in the BB sector from PSEA increases as BC passes through the Yunnan-Guizhou Plateau in China. The height of the highest value occurs at 2 km (approximately 800 hPa) when BC emitted from PSEA arrives at SC. This is why little surface BC is emitted from the BB sector over SC, while the proportion of BC in the BB sector increases to 10.3% of the total BCC in the air over SC. The BC contributed by SWC and ROW also increases with altitude. Bond et al. (2013) suggested that BC transported to higher altitudes is less likely to be removed and therefore has a longer lifetime, which is a favorable factor to enhance the BC RF. Hence, our results indicate that a considerable proportion of the BC RF over SC may be owing to the contributions of

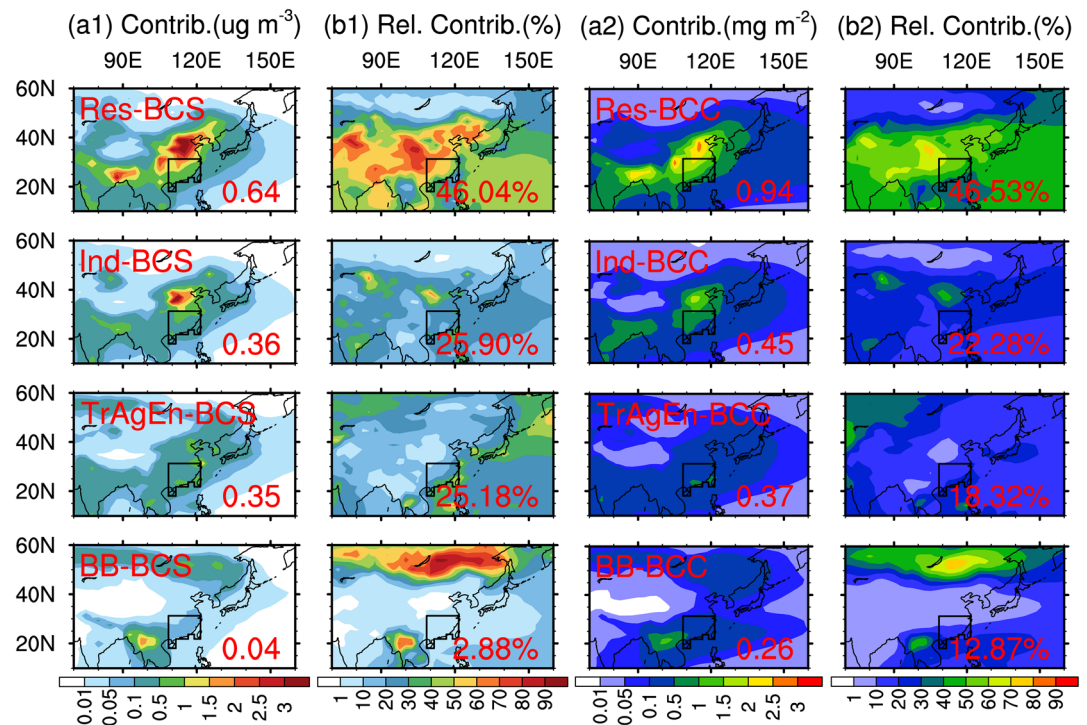


Figure 6. Spatial distributions of absolute contributions (units: $\mu\text{g m}^{-3}$; a1) and relative contributions (units: %; b1) to MAM mean BCS from different sectoral sources. (a2 and b2) The same as (a1) and (b1), respectively, but for absolute contributions (units: mg m^{-2} ; a2) and relative contributions (units: %; b2) to MAM mean BCC. The region enclosed by black lines represents SC. The averaged absolute and relative contributions of each sectoral source to BC over SC are given in the lower right corner of the panel.

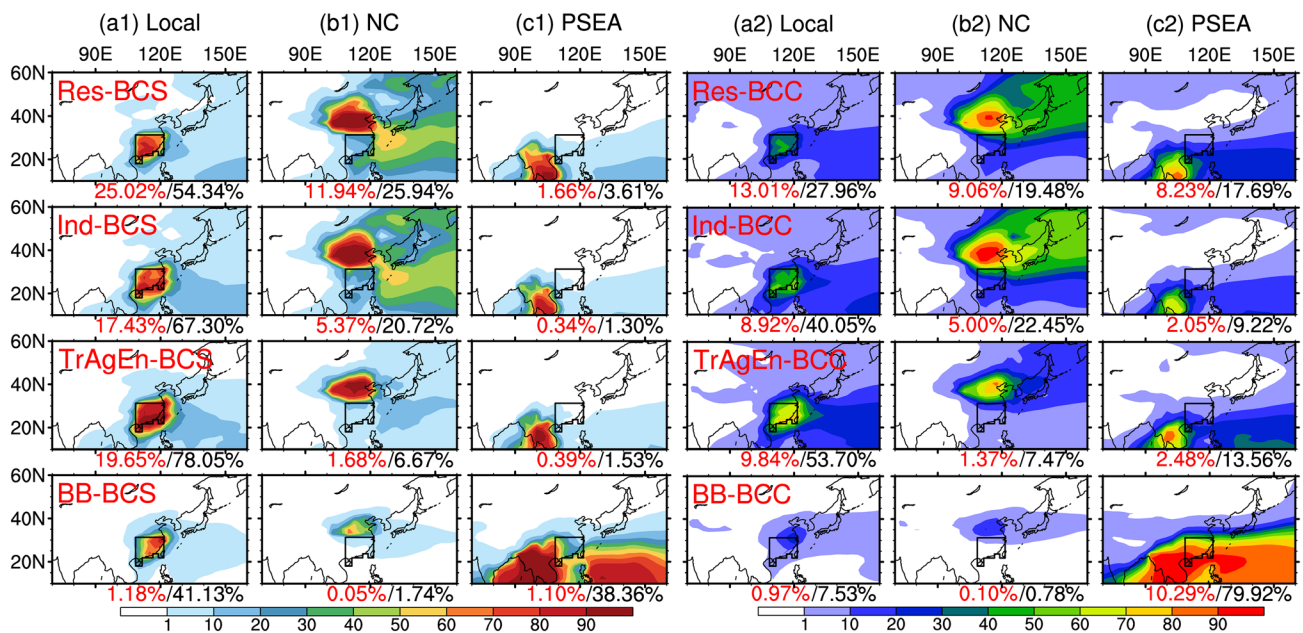


Figure 7. Spatial distributions of relative contributions (units: %) of Res, Ind, TrAgEn, and BB emission sectors from three tagged source regions (SC, NC, and PSEA) to MAM mean BC. (a1–c1) The relative contributions to BCS. (a2–c2) The relative contributions to BCC. The region enclosed by black lines represents SC. The proportions of BC originating from different emission sectors in the tagged source regions (SC, NC, and PSEA) to total BC averaged over SC are given in the lower right corner of the panels marked in red. The proportions of BC originating from different emission sectors in the tagged source regions (SC, NC, and PSEA) to BC in the corresponding sectors averaged over SC are given in the lower right corner of the panels marked in black.

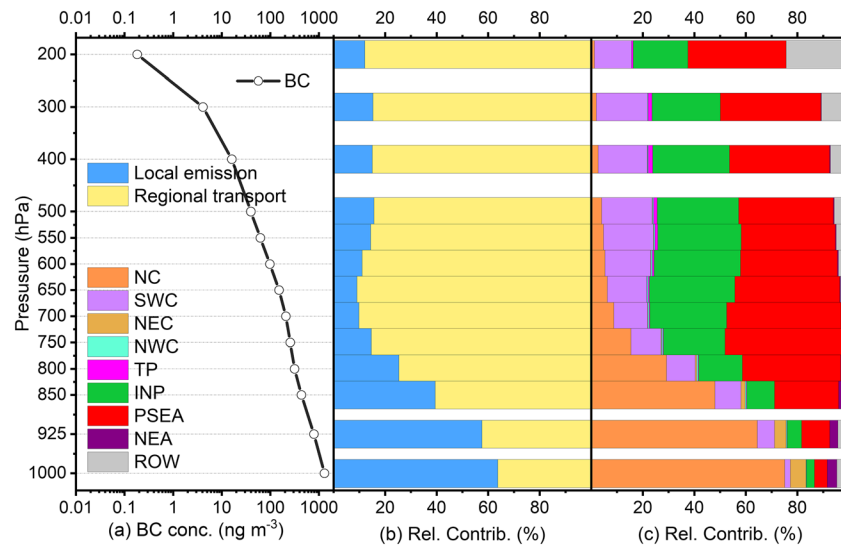


Figure 8. Vertical distributions of (a) MAM mean BC concentration (units: ng m^{-3}), (b) relative contributions (units: %) of local emission and regional transport to MAM mean BC concentration, and (c) relative contributions (units: %) of nonlocal sources to MAM mean BC concentration provided by regional transport over SC.

nonlocal sources, especially the contributions from non-China emissions (e.g., PSEA and INP). Further studies are needed to examine the above issue.

BC transported from NC may be mainly attributed to Res and Ind sources, as mentioned in the previous section. Figure 9 shows that BC from NC shares a similar compositional proportion at all altitudes, where 50–60% of BC is attributed to the Res sector, followed by the Ind sector (30–40%). Little BC emitted by the TrAgEn and BB sectors (below 5–8% and 0.5%, respectively) is transported from NC. Note that despite BC from PSEA and INP regions share the same primary transport layer, their sectoral compositions are not the same. The BC emitted in PSEA is mainly attributed to the BB sector (accounting for 50–60% below 600 hPa), followed by the Res and TrAgEn sectors (20–30% and 10%, respectively). Little BC transported from PSEA to SC is emitted in the Ind sector. INP mainly impacts BC over SC via the Res sector, followed by the Ind and TrAgEn sectors, whereas the proportion of the BB sector is small (accounting for 60%, 25%, 11%, and 3–5%, respectively). The BC transported in the troposphere from the other domestic regions is also mainly attributed to the Res sector (50–60%). The sectoral composition of BC from local SC emissions is slightly different from that of BC delivered from the other domestic regions. Locally emitted BC in the Res sector is dominant over SC, while its contribution to the total BC is approximately 10% lower than that from the other regions in China (40–50%) due to the increasing contribution of the TrAgEn sector (10% larger compared with other regions in China). Previous studies have highlighted the importance of transportation emissions to $\text{PM}_{2.5}$ in SC (Yin et al., 2017; Yu et al., 2018). The relative contribution of the TrAgEn sector to BC in SC is increased mainly due to the increased BC emissions from the local transportation sector. The BC transported from ROW to SC is mainly attributed to the TrAgEn sector (accounting for 40–60% below 600 hPa), which may be related to ship transportation in the coastal areas around SC.

3.5. Impacts of the Interannual Variation in EASM Onset Times on BC

3.5.1. Selection of the Years With Early/Late EASM Onset

The monsoon transition can be characterized as the reversal of wind direction or the alternation of dry and wet seasons (Zhao et al., 2007), and the time (or pentad) when the wind starts to reverse has been widely used to define the EASM onset time (He et al., 2008; Li & Pan, 2006; Wang, Zhu, et al., 2016). Wang, Zhu, et al. (2016) suggested that the meridional wind at 850 hPa can be used to assess the impacts induced by the varying EASM onset times on aerosols as aerosols are mainly distributed in the lower troposphere. In this study, the definition from He et al. (2008) and Wang, Zhu, et al. (2016) is followed to determine the establishment pentad of EASM over SC by the transition of meridional wind from northerly wind into southerly wind at 850 hPa in the subtropics (20–31.26°N, 108.75–121.25°E). The specific definition is as follows: (1) the onset

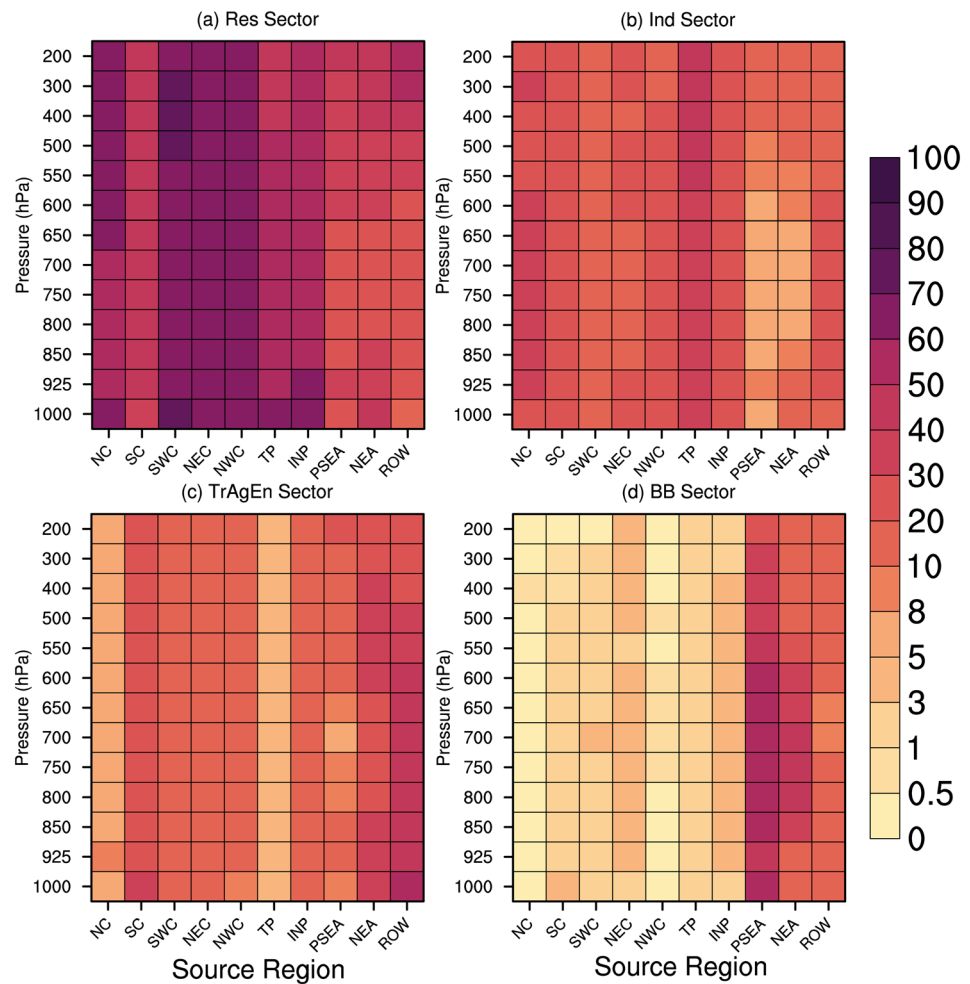


Figure 9. The sectoral compositions (Res, a; Ind, b; TrAgEn, c; and BB, d; units: %) of BC emitted from different source regions averaged over SC at different altitudes. Fractions in the corresponding boxes of the four panels add up to 100%.

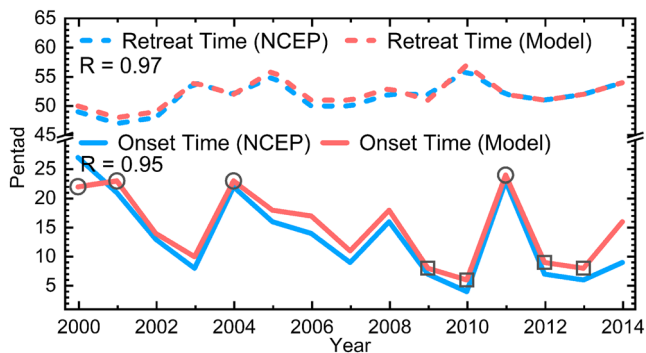


Figure 10. The EASM onset times (units: pentad, solid lines) and retreat times (units: pentad, dashed lines) over SC from the model results (red lines) and NCEP/NCAR reanalysis (blue lines) during 2000–2014. The selected years with early (square) or late (circle) EASM onset times and correlation coefficients (R) between the model results and NCEP/NCAR dataset are shown in the figure.

pentad of EASM is the pentad when the meridional wind at 850 hPa over SC starts to be greater than 0 m s^{-1} ($V_{850} > 0 \text{ m s}^{-1}$); (2) V_{850} remains greater than 0 m s^{-1} in the subsequent four pentads (including the onset pentad), or at least three pentads, and the average meridional wind speed of the accumulative four pentads is greater than 1.0 m s^{-1} ($V_{850} \geq 1.0 \text{ m s}^{-1}$); and (3) the retreat pentad of EASM is defined as the pentad when meridional wind turns negative ($V_{850} < 0 \text{ m s}^{-1}$).

Figure 10 gives the interannual variations in EASM onset and retreat times over SC during the simulation period calculated with the model result (MERRA) and National Centers for Environmental Prediction (NCEP)/National Center for Atmospheric Research (NCAR) reanalysis, respectively. The onset and retreat times using MERRA meteorological fields agree well with those based on NCEP/NCAR reanalysis ($R = 0.95$ and 0.97 , respectively). The establishment of EASM can also be characterized by the transition from dry continental climate to wet monsoon climate or the reversal of land-sea pressure contrast. EASM onset times

Table 1
Correlation Coefficients Among the EASM Onset Times Obtained Based on Different Definitions and Correlation Coefficients Between EASM Onset Times and Simulated BC Column Burden (Units: mg m^{-2} ; From Experiment $n_v\text{EMIS}$) Over SC During 2000–2014 Calculated From the Model Results, CMAP Precipitation Product, and NCEP/NCAR Reanalysis

Correlation coefficient	Model		CMAP and NCEP/NCAR	
	Onset time ^a	BC	Onset time ^a	BC
Onset time ^b	0.71**	0.42*	0.62**	0.29
Onset time ^c	0.52**	0.52**	0.52**	0.46*

^aThe EASM onset time defined by He et al. (2008) and Wang, Zhu, et al. (2016) is used in this study. ^bThe EASM onset time defined by Wang and Lin (2002) is determined by the difference between the pentad mean (R_i) and the January mean (R_{JAN}) precipitation rates ($RR_i = R_i - R_{JAN}$, $i = 1, 2, \dots, 73$). ^cThe EASM onset time defined by Guo (1983) is determined by the difference between the sea level pressures over 110°E ($SLP_{110^\circ E}$) and 160°E ($SLP_{160^\circ E}$) over East Asia (10–50°N) ($SLP_{diff, i} = SLP_{110^\circ E, i} - SLP_{160^\circ E, i}$, $i = 1, 2, \dots, 73$). **The correlation coefficient is statistically significant at the 0.05 level. *The correlation coefficient is statistically significant at the 0.1 level.

based on other definitions (Guo, 1983; Wang & Lin, 2002) were calculated with different feature factors (precipitation and sea level pressure). The temporal correlation coefficients (0.52–0.71) between the EASM onset time used in this study and EASM onset times calculated from other definitions based on the model results are statistically significant at the 0.05 level (Table 1). The EASM onset times obtained by different definitions in the NCEP/NCAR reanalysis and CPC Merged Analysis of Precipitation product (CMAP; <https://psl.noaa.gov/data/gridded/data.cmap.html>) also show strong correlations (0.52–0.62). These suggest the reliability of the definition of EASM onset time used in this study. To compare the impacts of the early or late EASM onset on the concentration and sources of BC over SC, we selected 4 years with the earliest EASM onset times (2009, 2010, 2012, and 2013) and 4 years with the latest onset times (2000, 2001, 2004, and 2011) during the simulation period, as shown in Figure 10. Table 2 shows that the average early/late EASM onset time is around the 8th/23rd pentad in this study. Similarly, Li and Zhang (2009) found that the seasonal reversal of the 850 hPa meridional winds happened from the 7th to 22nd pentad over SC. The difference in BC between the earliest/latest-year-average and 15-year average shows the influences of the early or late EASM onset on BC.

3.5.2. Changes in BC Concentration and Sources With Early/Late EASM Onset Time

From Figures 11a and 11c, it can be seen that the BC concentrations over SC and its surrounding areas change in an opposite way under the control of early or late EASM onset. The changes in BC concentrations are most significant over SC and NC. Figure 11a shows that the BC concentration over SC and its adjacent sea areas decreases when EASM onset is early while the BC concentration over NC increases at the same

Table 2
MAM Mean BC Column Burdens (Units: mg m^{-2}) in Early/Late EASM Onset Years and the Entire Simulation Period (2000–2014) Over SC and NC

Monsoon onset		Average onset time over SC (pentad)	BC conc. Avg. (mg m^{-2})	BC conc. Diff. (mg m^{-2})	BC conc. Diff. (%)
SC	Early	8th	1.91	−0.11	−5%
	Late	23rd	2.16	0.14	7%
	Average	15th	2.02		
	SD ^a		0.86		
NC	Early	8th	2.40	0.06	3%
	Late	23rd	2.20	−0.14	−6%
	Average	15th	2.34		
	SD		1.35		

Note. The average EASM onset times (units: pentad) in early/late EASM onset years and the entire simulation period (2000–2014) over SC are obtained following the definition of He et al. (2008) and Wang, Zhu, et al. (2016). The absolute difference (units: mg m^{-2}) and relative difference (units: %) between the MAM mean BC column burdens in early/late EASM onset years and the entire simulation period (2000–2014) over SC and NC are also shown.

^aSD represents the standard deviation of averaged BC column burden over the entire simulation period (2000–2014).

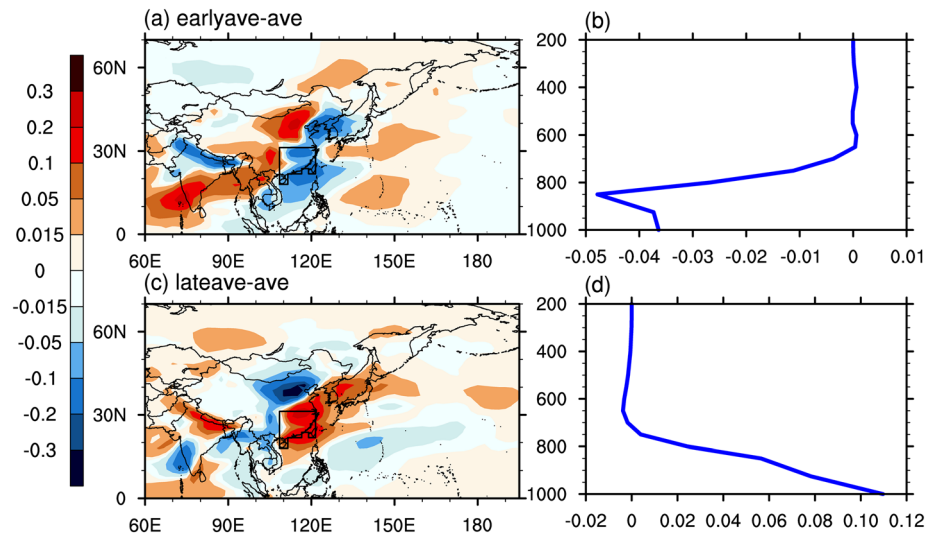


Figure 11. (a) Spatial distribution of the difference (units: mg m^{-2}) between the MAM mean BC column burden in early EASM onset years and that averaged from 2000 to 2014. (b) Same as (a), but for the vertical distribution of the BC difference (units: $\mu\text{g m}^{-3}$). (c and d) Same as (a) and (b), but for the difference between BC in late EASM onset years and that averaged from 2000 to 2014. The region wrapped with black lines represents SC. BC values are simulated from n_vEMIS.

time. However, late EASM onset time leads to an opposite change in BC concentrations in each region, manifesting as an increase in BC concentration over SC and adjacent areas but a decrease over NC. The maximum BC change over SC is near its northern edge, while the most significant change in BC over NC is generally consistent with the area with the strongest BC emission (figure not shown) and highest BC concentration (Figure 2) in MAM. Table 2 quantifies the difference in BCC between early/late EASM onset years and the entire simulation period (2000–2014) averaged over SC and NC. Compared with the BC concentration averaged from 2000 to 2014, BCC over SC is reduced by 5% (0.11 mg m^{-2}) when the EASM onset pentad is early. Meanwhile, the concentration of BCC over NC increases by 3% (0.06 mg m^{-2}). Late EASM onset causes even greater changes in BC concentrations. BCC over SC and NC areas increases/decreases by 0.14 mg m^{-2} , accounting for approximately 7% and 6% of their total BCC, respectively. Hence, the interannual variation in EASM onset can induce a maximum of -5% to $+7\%$ variation in BCC over SC during 2000–2014. The BCS variation induced by the interannual variation in EASM onset is basically the same as those of BCC but slightly smaller (Table S2). The resulting variation ranges of BCS over SC and NC are -2% to $+7\%$ and -2% to $+2\%$, respectively, when the EASM onset is relatively earlier or later. Mao et al. (2017) summarized the impacts of strongest and weakest EASM classified by the monsoon strength on the surface BC in East Asia. The variation in BCS over SC induced by varying EASM strength ranged from -5% to 5% , and the variation in BCS over NC ranged from -1% to -2% . In addition, with the variation in EAWM strength, the BCS in SC decreased or increased by 2%, while the BC in NC varied in the range of -2% to $+3\%$. Hence, the variations in EASM onset time and strength have comparable impacts on BC in magnitude.

The sources contributing to the variation in BC due to the early/late EASM onset are quantitatively revealed with the BC-tagging method. As shown in Figure 12, whether the EASM onset is early or late, the BC outflow/inflow transported from NC is the largest contributor to the variations in BC column burden over SC, surpassing the contribution of local inflow/outflow within SC. When the EASM is established relatively earlier, the BC provided by NC decreases by 0.07 mg m^{-2} , whereas the BC from NC increases by 0.10 mg m^{-2} inversely when the EASM establishment is later. The variation in BC contributed by other regions is not significant. It is mainly the difference in regional transport from NC that leads to the BCC variation over SC with the varying EASM onset times. The BC vertical changes given in Figures 11b and 11d further confirm this. The BC impacted by the interannual variation in EASM onset times is mainly distributed in the lower troposphere. Little impact on BC at higher altitudes (above 800 hPa) is exerted by the varying EASM onset times. The analysis in section 3.4 shows that the main transport layer of BC from NC is generally below

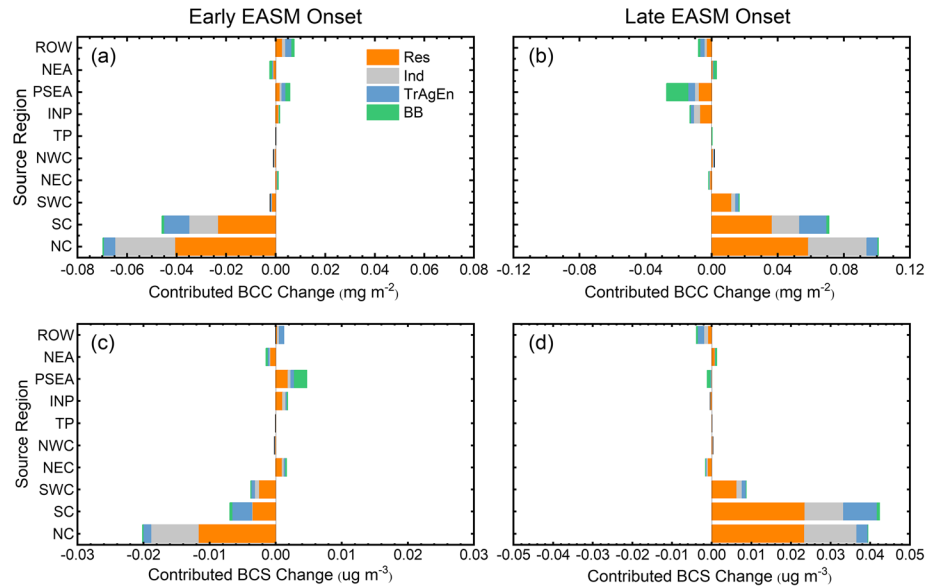


Figure 12. (a) Contribution (units: mg m^{-2}) from each tagged source region to the difference in BC column burden (BCC) over SC between early EASM onset years and the entire simulation period (2000–2014). Different colors in the bars represent the contributions of different emission sectors (Res, Ind, TrAgEn, and BB). (b) Same as (a), but for the contributions to the difference in BCC over SC between late EASM onset years and the entire simulation period (2000–2014). (c, d) Same as (a) and (b), respectively, but for contribution (units: $\mu\text{g m}^{-3}$) from each tagged source region to the difference in BC surface concentration (BCS) over SC.

850 hPa while most of the BC originating from PSEA and INP is transported in the middle and upper troposphere (Figure 8). Notably, the BC over SC transported from PSEA decreases by 0.03 mg m^{-2} due to the late EASM onset, accounting for 7.5% of the total contribution from PSEA. As for the variation in surface BC over SC, BC increase provided by local emissions slightly exceeds the contribution of the BC inflow transported from NC when EASM is established relatively later. But overall, most of the variation in BCS induced by early/late EASM onset can be attributed to the difference in regional transport from NC. Figure 13 gives the advective tendency anomalies of BC emitted from NC and wind field anomalies at 850 hPa when the EASM onset time is relatively earlier or later. The positive value indicates a net inflow of BC transported from NC, and the negative value represents a net outflow. When the EASM onset pentad is early (late), the southerly (northerly) wind anomaly prevails in eastern China, which blocks (promotes) the southward transport of BC provided by NC. Therefore, the BC inflow from NC to SC is negative (positive), while the inflow over NC itself is positive (negative). The variation in BC concentrations over SC impacted by EASM onset time is dominated by the regional transport from NC, thus leading to a decreasing (increasing) trend in BC over the SC region.

Figure 14 gives the interannual variations in BC concentrations, EASM onset times and BC emissions averaged over SC. The time series of BC emissions in the BB sector from PSEA is also provided. The interannual variation in BC concentrations agrees well with that of the EASM onset times without the impacts of emission factor (experiment n_vEMIS), showing a significant positive correlation ($R = 0.66, p < 0.05$) in Figure 14a. This indicates that the earlier the EASM is established, the lower the BC concentration is over SC. Table 1 also shows the positive correlation coefficients (0.42–0.52) between the EASM onset times defined in other studies and BC concentrations. Notably, the correlation between BC concentrations and emissions over SC is not significant when emission and meteorological factors are both taken into consideration (Figure 14b), whereas the BC concentrations are still positively correlated with the EASM onset times ($R = +0.62, p < 0.05$; Figure 14a). Moreover, a significant correlation coefficient of 0.51 is found between the BC concentrations over SC and the BC emissions in the BB sector from PSEA (Figure 14b). The standard deviation (0.02) of the BC interannual variation induced by the variation in BB emissions from PSEA over SC

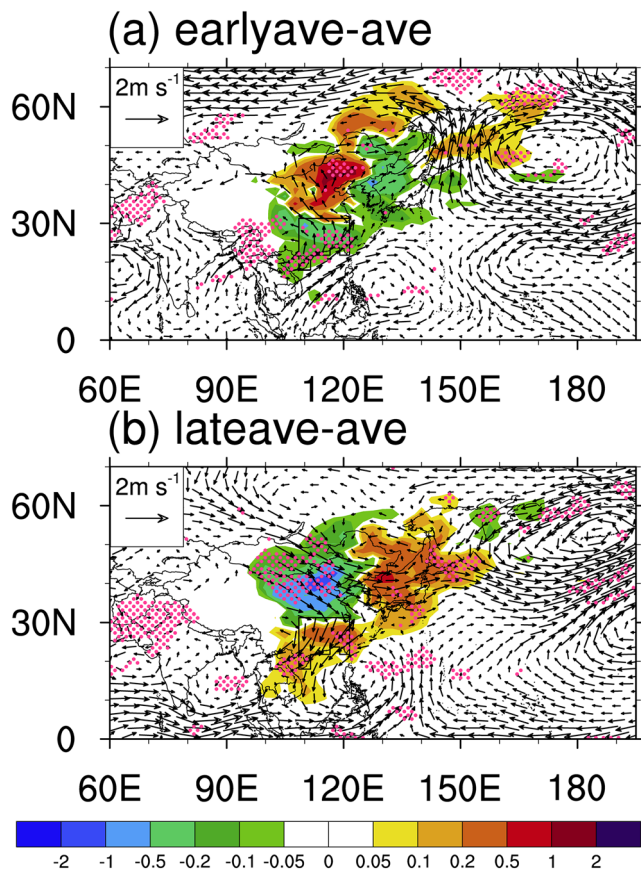


Figure 13. (a) Composite MAM mean advective tendency anomaly of BC originating from NC (unit: $10^{-6} \text{ mg m}^{-2} \text{ s}^{-1}$, contours) and MAM mean 850 hPa wind direction anomaly (unit: m s^{-1} , vectors) in early EASM onset years. (b) Same as (a), but for the anomalies in late EASM onset years. The dot signs denote where the anomaly is statistically significant at the 0.05 level.

is much smaller than that (0.86 in Table 2) induced by the variation in EASM onset times. The above results indicate that the interannual variation in BC concentrations over SC during springtime is mainly controlled by meteorological factors in recent years. The relationship between BC concentrations and EASM retreat times in SON is also examined in Figure S8, which shows a significant negative correlation coefficient ($R = -0.64, p < 0.05$). The BC concentration over SC is relatively high in SON when EASM retreat is early, which is similar to the relationship between the EASM onset times and BC concentrations over SC in MAM. Unlike the condition in MAM, BC concentration in SON is significantly correlated with the BC emissions over SC ($R = +0.49, p < 0.05$), suggesting that the interannual variation in BC concentrations over SC in SON is influenced jointly by the emission and meteorological factors.

3.6. Uncertainties

The results of the BC-tagging technique highly depend on the model performance in reproducing the BC distribution and evolution. Through multiple comparisons, we examined that the model well captures the spatial coverage and interannual temporal evolution of BC over SC. However, the general underestimation of simulated BC is found in this study, leading to the bias in the absolute contributions of source regions and sectors to BC over SC. The underestimation of simulated BC also exists in previous studies and can be attributed to several factors (Bond et al., 2013; Jiang et al., 2013; Yang et al., 2017, 2018; Zhang, Wang, Hegg, et al., 2015; Zhang, Wang, Qian, et al., 2015). The coarse resolution used in global models are unable to consider the subgrid aerosol variability (Qian et al., 2010). For example, emissions in model are uniformly distributed over a grid cell volume, while the spatial distribution of BC emissions may come from point, area, and mobile sources and are inhomogeneous within a model grid cell. Model grid-averaged output also results in the negative bias of model results compared to observations sampled at individual point sites.

Additionally, BC emissions are subject to uncertainty in existing inventories. Using the anthropogenic emissions from PKU-BC inventory with a subnational fuel consumption data and updated emission factor measurements and daily BB emissions from GFED v4.1s, the bias (-26%) of MAM mean BC in China simulated in this study is reduced compared with the simulation results (-53% to -51%) based on other inventories. However, compared to the BC emissions constrained by the observations of BC light absorption from Bond et al. (2013), there still exists biases in the BC emissions in East Asia (-26%), South Asia (-67%), Southeast Asia (-68%), and other regions (-83 to 11%) from PKU-BC (Wang, Tao, Shen, et al., 2014). Note that Wang, Rasch, Easter, et al. (2014) showed that the distributions of tagged BC mixing ratio and deposition changes from individual sources are nearly linear when BC emissions are perturbed. Therefore, underestimation may exist in the results of absolute contributions of source regions and sectors to BC over SC due to the uncertainty in BC emissions; besides, the relative contributions of non-China emissions, especially from INP and PSEA, may be underestimated considering the larger biases of BC emissions in South and Southeast Asia than in East Asia from PKU-BC.

Note that the BC aging timescale is fixed (1.6 days) in MOZART-4 although it may vary in different regions in reality. Previous studies indicated that the aging timescale of anthropogenic BC from East Asia could be several hours (faster than assumed in most global models), while the aging process of BC originating from BB emissions in Southeast Asia may be slower, with a timescale of a few days (Shen et al., 2014; Zhang, Liu, Tao, & Ban-Weiss, 2015). Zhang, Liu, Tao, & Ban-Weiss (2015) found that the lifetime of BC increases nearly linearly with aging timescale for all source regions, indicating the slower removal of BC with longer aging timescale during transport. Hence, the bias in BC aging timescale may also produce an underestimation of contribution from PSEA to BC over SC in this study. However, results from Wang, Rasch, Easter,

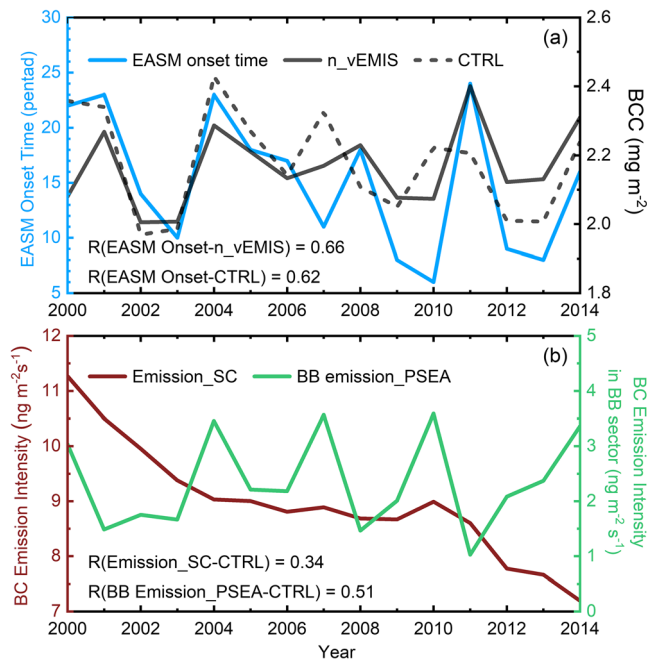


Figure 14. Time series of BC column burden (BCC, units: mg m^{-2} , black solid and dashed lines in panel a), EASM onset time (units: pentad, blue line in panel a) and BC emission intensity (units: $\text{ng m}^{-2} \text{s}^{-1}$, brown line in panel b) over SC and the BC emission intensity from BB sector over PSEA (units: $\text{ng m}^{-2} \text{s}^{-1}$, green line in panel b) during 2000–2014. The BC concentrations represented by black solid and dashed lines in (a) are simulated from n_vEMIS and CTRL, respectively.

et al. (2014) showed that the BC aging treatment brings small change in the source-receptor relationships. Moreover, our results for the relative contributions to BC are qualitatively consistent with those of previous studies using observational and/or modeling approaches (Chan, 2017; Li, Liao, et al., 2016; Yang et al., 2017; Zhang et al., 2014).

4. Conclusions

The BC-tagging technique applied in CESM in this study is a useful tool for tracking BC sources by region and by sector without perturbing emissions. We quantified the region-based and sector-based contributions to BC and examined the long-term impacts of biomass burning (BB) emissions originating from peninsula Southeast Asia (PSEA) on South China (SC) during springtime. Furthermore, the East Asian summer monsoon (EASM) is established in spring when the wind direction begins to reverse. SC is under the control of the East Asian subtropical monsoon system, and the time when EASM is established impacts the BC distribution and transport. Hence, the interannual variations in BC concentrations and sources influenced by the variation in EASM onset times were investigated with the BC-tagging technique.

In our work, a large amount of BC is transported from PSEA and the Indian peninsula (INP) and increases the BC concentration at high altitudes over SC. Most of the BC column burden emitted from BB sector (~80%) over SC can be attributed to regional transport from PSEA during 2000–2014. The high BB emissions in PSEA increase the total BC column burden over SC by 10.3%. This increase could be even larger if vertical-variant BB emissions associated with plume injection are considered. Given the higher RF efficiency (RF exerted per gram of BC; Samset et al., 2013,

2014) and longer lifetime (Bond et al., 2013) of BC at higher altitudes, further studies are needed to examine the potential large contributions of BB emissions to the direct BC RF over SC.

In contrast to the large contributions of non-China emissions to BC at high altitudes, the anthropogenic emissions from North China (NC) are the dominant nonlocal contributor to BC in the lower troposphere over SC (contributing 17.3% of the BC surface concentration). Moreover, through tracking the specific sources of the variation in BC induced by the interannual variation in EASM onset times with the emission-fixed experiment, the BC variation due to the different EASM onset times over SC is found to be controlled by the BC outflow/inflow contributed from NC. A southerly wind anomaly occurs over East Asia and blocks the southward transport of BC from NC to SC due to the early EASM onset. Therefore, BC is difficult to be exported from NC, and the BC concentration over SC provided by NC is thus reduced. In the year with late EASM onset, this pattern is reversed. The results show that the BC changes over SC and NC represent opposite characteristics. The BC concentration over SC decreases by 0.11 mg m^{-2} (increases by 0.14 mg m^{-2}), while the BC concentration over NC increases by 0.06 mg m^{-2} (decreases by 0.14 mg m^{-2}) when the EASM onset is early (late). The role of meteorological and emission factors on the interannual variations of BC in spring are further examined. The simulated MAM BC concentrations averaged over SC exhibit strong positive correlation with the EASM onset times both in the emission-fixed experiment ($R = +0.66$) and the control experiment ($R = +0.62$). However, no significant correlation is found between the BC concentrations and emissions during 2000–2014, indicating that the interannual variation in BC concentrations over SC during springtime in recent years is mainly controlled by meteorological factors.

Note that the impacts of the variation in EASM onset times on BC in spring we evaluate are as important as the impacts of the variation in EASM and EAWM strengths on BC given in previous studies, but the former is less discussed. Further studies need to be conducted on how the establishment and retreat of EASM in spring and autumn impact BC and other aerosols. Moreover, this study mainly investigates the impacts of the interannual variation in EASM onset times on BC by altering the wind field. Other meteorological

factors (precipitation, etc.) affected by the varying EASM onset times can also adjust the BC horizontal and vertical distributions and should be considered in the future.

In summary, regional transport from the nonlocal source regions inside and outside China leads to an increase in the BC concentrations at different altitudes over SC in MAM. The BC transported from NC controls the BC variation over SC induced by the interannual variation in EASM onset. The BC sources over NC are also investigated here. NC is recognized as another highly polluted area in China, but regional transport has little impact on BC from the surface to the upper air (Table S3), which differs from the situation over SC.

Conflict of Interest

The authors declare no competing financial interests.

Data Availability Statement

The CESM code is available online (https://svn-ccsm-release.cgd.ucar.edu/model_versions/). The Peking University BC inventory is available online (<http://inventory.pku.edu.cn/home.html>). The GFEDv4 database is available online (https://daac.ornl.gov/VEGETATION/guides/fire_emissions_v4_R1.html). The MERRA and MERRA-2 reanalysis are available from <https://www.earthsystemgrid.org/dataset/ucar.cgd.cesm.4.merra.html> and <https://disc.gsfc.nasa.gov/datasets?page=1&keywords=MERRA-2> websites, respectively. The NCEP/NCAR reanalysis is available online (<https://psl.noaa.gov/data/gridded/data.ncep.reanalysis.html>). The CMAP product is available online (<https://psl.noaa.gov/data/gridded/data.cmap.html>).

Acknowledgments

This work is supported by grants from the National Key Research and Development Program of China (2016YFA0602003) and the National Natural Science Foundation of China (41805120, 42021004). Thanks Delong Zhao (Beijing Weather Modification Office) for providing BC profile data.

References

- Babu, S. S., & Moorthy, K. K. (2002). Aerosol black carbon over a tropical coastal station in India. *Geophysical Research Letters*, *29*(23), 2098. <https://doi.org/10.1029/2002GL015662>
- Begam, G. R., Vachaspati, C. V., Ahammed, Y. N., Kumar, K. R., Babu, S. S., & Reddy, R. R. (2016). Measurement and analysis of black carbon aerosols over a tropical semi-arid station in Kadapa, India. *Atmospheric Research*, *171*, 77–91. <https://doi.org/10.1016/j.atmosres.2015.12.014>
- Bey, I., Jacob, D. J., Logan, J. A., & Yantosca, R. M. (2001). Asian chemical outflow to the Pacific in spring: Origins, pathways, and budgets. *Journal of Geophysical Research*, *106*(D19), 23,097–23,113. <https://doi.org/10.1029/2001JD000806>
- Bollasina, M. A., Ming, Y., & Ramaswamy, V. (2013). Earlier onset of the Indian monsoon in the late twentieth century: The role of anthropogenic aerosols. *Geophysical Research Letters*, *40*, 3715–3720. <https://doi.org/10.1002/grl.50719>
- Bond, T. C., Doherty, S. J., Fahey, D., Forster, P., Berntsen, T., DeAngelo, B., et al. (2013). Bounding the role of black carbon in the climate system: A scientific assessment. *Journal of Geophysical Research: Atmospheres*, *118*, 5380–5552. <https://doi.org/10.1002/jgrd.50171>
- Bond, T. C., Streets, D. G., Yarber, K. F., Nelson, S. M., Woo, J. H., & Klimont, Z. (2004). A technology-based global inventory of black and organic carbon emissions from combustion. *Journal of Geophysical Research*, *109*, D14203. <https://doi.org/10.1029/2003JD003697>
- Chan, K. L. (2017). Biomass burning sources and their contributions to the local air quality in Hong Kong. *The Science of the Total Environment*, *596–597*, 212–221. <https://doi.org/10.1016/j.scitotenv.2017.04.091>
- Chen, H. P., & Wang, H. J. (2015). Haze days in North China and the associated atmospheric circulations based on daily visibility data from 1960 to 2012. *Journal of Geophysical Research: Atmospheres*, *120*, 5895–5909. <https://doi.org/10.1002/2015JD023225>
- Chen, S. F., Guo, J. P., Song, L. Y., Li, J., Liu, L., & Cohen, J. B. (2018). Inter-annual variation of the spring haze pollution over the North China Plain: Roles of atmospheric circulation and sea surface temperature. *International Journal of Climatology*, *39*(2), 783–798. <https://doi.org/10.1002/joc.5842>
- Cheng, Y., Lee, S. C., Ho, K. F., Wang, Y. Q., Cao, J. J., Chow, J. C., & Watson, J. G. (2006). Black carbon measurement in a coastal area of South China. *Journal of Geophysical Research*, *111*, D12310. <https://doi.org/10.1029/2005JD006663>
- Cohen, D. D., Crawford, J., Stelcer, E., & Bac, V. T. (2010). Characterisation and source apportionment of fine particulate sources at Hanoi from 2001 to 2008. *Atmospheric Environment*, *44*(3), 320–328. <https://doi.org/10.1016/j.atmosenv.2009.10.037>
- Cooke, W. F., & Wilson, J. J. (1996). A global black carbon aerosol model. *Journal of Geophysical Research*, *101*(D14), 19,395–19,409. <https://doi.org/10.1029/96JD00671>
- Deng, X., Tie, X., Zhou, X., Wu, D., Zhong, L., Tan, H., et al. (2008). Effects of Southeast Asia biomass burning on aerosols and ozone concentrations over the Pearl River Delta (PRD) region. *Atmospheric Environment*, *42*(36), 8493–8501. <https://doi.org/10.1016/j.atmosenv.2008.08.013>
- Ding, A. J., Huang, X., Nie, W., Sun, J. N., Kerminen, V. M., Petäjä, T., et al. (2016). Enhanced haze pollution by black carbon in megacities in China. *Geophysical Research Letters*, *43*, 2873–2879. <https://doi.org/10.1002/2016GL067745>
- Emmons, L. K., Walters, S., Hess, P. G., Lamarque, J.-F., Pfister, G. G., Fillmore, D., et al. (2010). Description and evaluation of the Model for Ozone and Related chemical Tracers, version 4 (MOZART-4). *Geoscientific Model Development*, *3*(1), 43–67. <https://doi.org/10.5194/gmd-3-43-2010>
- Fu, G. Q., Xu, W. Y., Yang, R. F., Li, J. B., & Zhao, C. S. (2014). The distribution and trends of fog and haze in the North China Plain over the past 30 years. *Atmospheric Chemistry Physics*, *14*(21), 11,949–11,958. <https://doi.org/10.5194/acp-14-11949-2014>
- Fu, J. S., Hsu, N. C., Gao, Y., Huang, K., Li, C., Lin, N. H., & Tsay, S. C. (2012). Evaluating the influences of biomass burning during 2006 BASE-ASIA: A regional chemical transport modeling. *Atmospheric Chemistry Physics*, *12*(9), 3837–3855. <https://doi.org/10.5194/acp-12-3837-2012>
- Gao, J., Zhu, B., Xiao, H., Kang, H., Pan, C., Wang, D., & Wang, H. (2018). Effects of black carbon and boundary layer interaction on surface ozone in Nanjing, China. *Atmospheric Chemistry Physics*, *18*(10), 7081–7094. <https://doi.org/10.5194/acp-2017-1177>

- Gelaro, R., McCarty, W., Suárez, M. J., Todling, R., Molod, A., Takacs, L., et al. (2017). The Modern-Era Retrospective analysis for Research and Applications, version 2 (MERRA-2). *Journal of Climate*, *30*(14), 5419–5454. <https://doi.org/10.1175/JCLI-D-16-0758.1>
- Guo, Q. Y. (1983). The strength index of East Asian summer monsoon and its variation. Chinese. *Acta Geographica Sinica*, *50*(3), 207–217. [in Chinese]. <https://doi.org/10.11821/xb198303001>
- Guo, S., Hu, M., Zamora, M. L., Peng, J., & Zhang, R. (2014). Elucidating severe urban haze formation in China. *Proceedings of the National Academy of Sciences*, *111*(49), 17,373–17,378. <https://doi.org/10.1073/pnas.1419604111>
- He, J. H., Zhao, P., Zhu, C. W., Zhang, R. H., Tang, X., Chen, L. X., & Zhou, X. J. (2008). Discussion of some problems as to the East Asian subtropical monsoon. *Journal of Meteorological Research*, *113*(D1), 419–434. <https://doi.org/10.1029/2007JD008874>
- Holtlag, A. A. M., & Boville, B. A. (1993). Local versus nonlocal boundary-layer diffusion in a global climate model. *Journal of Climate*, *6*(10), 1825–1842. [https://doi.org/10.1175/1520-0442\(1993\)006<1825:LVNBLD>2.0.CO;2](https://doi.org/10.1175/1520-0442(1993)006<1825:LVNBLD>2.0.CO;2)
- Horowitz, L. W., Walters, S., Mauzerall, D. L., Emmons, L. K., Rasch, P. J., Granier, C., et al. (2003). A global simulation of tropospheric ozone and related tracers: Description and evaluation of MOZART, version 2. *Journal of Geophysical Research*, *108*(D24), 4784. <https://doi.org/10.1029/2002JD002853>
- Huang, K., Fu, J. S., Hsu, N. C., Gao, Y., Dong, X., Tsay, S. C., & Lam, Y. F. (2013). Impact assessment of biomass burning on air quality in Southeast and East Asia during BASE-ASIA. *Atmospheric Environment*, *78*, 291–302. <https://doi.org/10.1016/j.atmosenv.2012.03.048>
- Hurrell, J. W., Holland, M. M., Gent, P. R., Ghan, S., Kay, J. E., Kushner, P. J., et al. (2013). The Community Earth System Model: A framework for collaborative research. *Bulletin of the American Meteorological Society*, *94*(9), 1339–1360. <https://doi.org/10.1175/BAMS-D-12-00121.1>
- Jacobson, M. Z. (2002). Control of fossil-fuel particulate black carbon and organic matter, possibly the most effective method of slowing global warming. *Journal of Geophysical Research*, *107*(D19), 4410. <https://doi.org/10.1029/2001JD001376>
- Jiang, Y. Q., Liu, X. H., Yang, X. Q., & Wang, M. H. (2013). A numerical study of the effect of different aerosol types on East Asian summer clouds and precipitation. *Atmospheric Environment*, *70*, 51–63. <https://doi.org/10.1016/j.atmosenv.2012.12.039>
- Joshi, H., Naja, M., Singh, K. P., Kumar, R., Bhardwaj, P., Babu, S. S., et al. (2016). Investigations of aerosol black carbon from a semi-urban site in the Indo-Gangetic Plain region. *Atmospheric Environment*, *125*, 346–359. <https://doi.org/10.1016/j.atmosenv.2015.04.007>
- Kalluri, R. O. R., Gugamsetty, B., Kotalo, R. G., Nagireddy, S. K. R., Tandule, C. R., Thotli, L. R., et al. (2017). Seasonal variation of near surface black carbon and satellite derived vertical distribution of aerosols over a semi-arid station in India. *Atmospheric Research*, *184*, 77–87. <https://doi.org/10.1016/j.atmosres.2016.09.003>
- Kwok, R. H., Fung, J. C., Lau, A. K., & Fu, J. S. (2010). Numerical study on seasonal variations of gaseous pollutants and particulate matters in Hong Kong and Pearl River Delta Region. *Journal of Geophysical Research*, *115*, D16308. <https://doi.org/10.1029/2009JD012809>
- Lamarque, J. F., Emmons, L. K., Hess, P. G., Kinnison, D. E., Tilmes, S., Vitt, F., et al. (2012). CAM-chem: Description and evaluation of interactive atmospheric chemistry in the Community Earth System Model. *Geoscientific Model Development*, *5*(2), 369–411. <https://doi.org/10.5194/gmd-5-369-2012>
- Lan, Z. J., Huang, X. F., Yu, K. Y., Sun, T. L., Zeng, L. W., & Hu, M. (2013). Light absorption of black carbon aerosol and its enhancement by mixing state in an urban atmosphere in South China. *Atmospheric Environment*, *69*, 118–123. <https://doi.org/10.1016/j.atmosenv.2012.12.009>
- Lauritzen, P. H., Ullrich, P. A., & Nair, R. D. (2011). Atmospheric transport schemes: Desirable properties and a semi-Lagrangian view on finite-volume discretizations. In P. H. Lauritzen (Ed.), *Numerical Techniques for Global Atmospheric Models* (pp. 185–251). Berlin: Springer. https://doi.org/10.1007/978-3-642-11640-7_8
- Li, B., Gasser, T., Ciais, P., Piao, S., Tao, S., Balkanski, Y., et al. (2016). The contribution of China's emissions to global climate forcing. *Nature*, *531*(7594), 357–361. <https://doi.org/10.1038/nature17165>
- Li, C. Y., & Pan, J. (2006). Atmospheric circulation characteristics associated with the onset of Asian summer monsoon. *Advances in Atmospheric Sciences*, *23*(6), 925–939. <https://doi.org/10.1007/s00376-006-0925-1>
- Li, J. P., & Zeng, Q. C. (2003). A new monsoon index and the geographical distribution of the global monsoons. *Advances in Atmospheric Sciences*, *20*(2), 299–302. <https://doi.org/10.1007/s00376-003-0016-5>
- Li, J. P., & Zhang, L. (2009). Wind onset and withdrawal of Asian summer monsoon and their simulated performance in AMIP models. *Climate Dynamics*, *32*(7–8), 935–968. <https://doi.org/10.1007/s00382-008-0465-8>
- Li, K., Liao, H., Mao, Y., & Ridley, D. A. (2016). Source sector and region contributions to concentration and direct radiative forcing of black carbon in China. *Atmospheric Environment*, *124*, 351–366. <https://doi.org/10.1016/j.atmosenv.2015.06.014>
- Li, M., Zhang, Q., Kurokawa, J. I., Woo, J. H., He, K., Lu, Z., et al. (2017). MIX: A mosaic Asian anthropogenic emission inventory under the international collaboration framework of the MICS-Asia and HTAP. *Atmospheric Chemistry Physics*, *17*(2), 935–963. <https://doi.org/10.5194/acp-17-935-2017>
- Li, Q., Zhang, R., & Wang, Y. (2016). Interannual variation of the wintertime fog-haze days across central and eastern China and its relation with East Asian winter monsoon. *International Journal of Climatology*, *36*(1), 346–354. <https://doi.org/10.1002/joc.4350>
- Lin, N. H., Tsay, S. C., Maring, H. B., Yen, M. C., Sheu, G. R., Wang, S. H., et al. (2013). An overview of regional experiments on biomass burning aerosols and related pollutants in Southeast Asia: From BASE-ASIA and the Dongsha Experiment to 7-SEAS. *Atmospheric Environment*, *78*, 1–19. <https://doi.org/10.1016/j.atmosenv.2013.04.066>
- Luo, M., & Lin, L. J. (2017). Objective determination of the onset and withdrawal of the South China Sea summer monsoon. *Atmospheric Science Letters*, *18*(6), 276–282. <https://doi.org/10.1002/asl.753>
- Mao, Y. H., Liao, H., & Chen, H. S. (2017). Impacts of East Asian summer and winter monsoons on interannual variations of mass concentrations and direct radiative forcing of black carbon over eastern China. *Atmospheric Chemistry Physics*, *17*(7), 4799–4816. <https://doi.org/10.5194/acp-17-4799-2017>
- Matsui, H., Koike, M., Kondo, Y., Oshima, N., Moteki, N., Kanaya, Y., et al. (2013). Seasonal variations of Asian black carbon outflow to the Pacific: Contribution from anthropogenic sources in China and biomass burning sources in Siberia and Southeast Asia. *Journal of Geophysical Research: Atmospheres*, *118*, 9948–9967. <https://doi.org/10.1002/jgrd.50702>
- Meng, J., Liu, J., Yi, K., Yang, H., Guan, D., Liu, Z., et al. (2018). Origin and radiative forcing of black carbon aerosol: Production and consumption perspectives. *Environmental Science & Technology*, *52*(11), 6380–6389. <https://doi.org/10.1021/acs.est.8b01873>
- Menon, S., Hansen, J., Nazarenko, L., & Luo, Y. (2002). Climate effects of black carbon aerosols in China and India. *Science*, *297*(5590), 2250–2253. <https://doi.org/10.1126/science.1075159>
- Neale, R. B., Chen, C.-C., Gettelman, A., Lauritzen, P. H., Park, S., Williamson, D. L., et al. (2012). *Description of the NCAR Community Atmosphere Model (CAM 5.0) (NCAR Tech. Note NCAR/TN-486+STR)*. Boulder, Colorado, USA: National Center for Atmospheric Research.

- Niu, F., Li, Z., Li, C., Lee, K.-H., & Wang, M. (2010). Increase of wintertime fog in China: Potential impacts of weakening of the Eastern Asian monsoon circulation and increasing aerosol loading. *Journal of Geophysical Research*, *115*, D00K20. <https://doi.org/10.1029/2009JD013484>
- Ohara, T., Akimoto, H., Kurokawa, J., Horii, N., Yamaji, K., Yan, X., & Hayasaka, T. (2007). An Asian emission inventory of anthropogenic emission sources for the period 1980–2020. *Atmospheric Chemistry Physics*, *7*(16), 4419–4444. <https://doi.org/10.5194/acp-7-4419-2007>
- Pan, C., Zhu, B., Gao, J., & Kang, H. (2017). Source apportionment of atmospheric water over East Asia—a source tracer study in CAM5.1. *Geoscientific Model Development*, *10*(2), 673–688. <https://doi.org/10.5194/gmd-10-673-2017>
- Park, S., & Bretherton, C. S. (2009). The University of Washington shallow convection and moist turbulence schemes and their impact on climate simulations with the Community Atmosphere Model. *Journal of Climate*, *22*(12), 3449–3469. <https://doi.org/10.1175/2008JCLI2557.1>
- Qi, L., He, J. H., Zhang, Z. Q., & Song, J. N. (2007). The seasonal reversal of zonal land-sea thermal contrast in relation to eastern Asian tropical monsoon circulation. *Chinese Science Bulletin*, *52*(24), 2895–2899. [in Chinese]. <https://doi.org/10.1360/CSB2007-52-24-2895>
- Qian, Y., Gustafson, W. L., & Fast, J. D. (2010). An investigation of the sub-grid variability of trace gases and aerosols for global climate modeling. *Atmospheric Chemistry Physics*, *10*(14), 6917–6946. <https://doi.org/10.5194/acp-10-6917-2010>
- Qin, Y., & Xie, S. D. (2012). Spatial and temporal variation of anthropogenic black carbon emissions in China for the period 1980–2009. *Atmospheric Chemistry Physics*, *12*(11), 4825–4841. <https://doi.org/10.5194/acp-12-4825-2012>
- Ramaswamy, V., Boucher, O., Haigh, J., Hauglustine, D., Haywood, J., Myhre, G., et al. (2001). Radiative forcing of climate change. In J. T. Houghton, et al. (Eds.), *Climate change 2001: The scientific basis* (pp. 349–416). Cambridge, UK: Intergovernmental Panel on Climate Change, Cambridge University Press.
- Randerson, J. T., Van Der Werf, G. R., Giglio, L., Collatz, G. J., & Kasibhatla, P. S. (2017). Global Fire Emissions Database, version 4.1 (GFEDv4). ORNL distributed active archive center. <https://doi.org/10.3334/ORNLDAAAC/1293>
- Rasch, P. J., Coleman, D. B., Mahowald, N., Williamson, D. L., Lin, S. J., Boville, B. A., & Hess, P. (2006). Characteristics of atmospheric transport using three numerical formulations for atmospheric dynamics in a single GCM framework. *Journal of Climate*, *19*(11), 2243–2266. <https://doi.org/10.1175/JCLI3763.1>
- Richter, J. H., & Rasch, P. J. (2008). Effects of convective momentum transport on the atmospheric circulation in the Community Atmosphere Model, version 3. *Journal of Climate*, *21*(7), 1487–1499. <https://doi.org/10.1175/2007JCLI1789.1>
- Rienecker, M. M., Suarez, M. J., Gelaro, R., Todling, R., Bacmeister, J., Liu, E., et al. (2011). MERRA: NASA's modern-era retrospective analysis for research and applications. *Journal of Climate*, *24*(14), 3624–3648. <https://doi.org/10.1175/JCLI-D-11-00015.1>
- Rotman, D. A., Atherton, C. S., Bergmann, D. J., Cameron-Smith, P. J., Chuang, C. C., Connell, P. S., et al. (2004). IMPACT, the LLNL 3-D global atmospheric chemical transport model for the combined troposphere and stratosphere: Model description and analysis of ozone and other trace gases. *Journal of Geophysical Research*, *109*, D04303. <https://doi.org/10.1029/2002JD003155>
- Sadiq, M., Tao, W., Liu, J., & Tao, S. (2015). Air quality and climate responses to anthropogenic black carbon emission changes from East Asia, North America and Europe. *Atmospheric Environment*, *120*, 262–276. <https://doi.org/10.1016/j.atmosenv.2015.07.001>
- Sahu, L. K., Kondo, Y., Miyazaki, Y., Pongkiatkul, P., & Kim Oanh, N. T. (2011). Seasonal and diurnal variations of black carbon and organic carbon aerosols in Bangkok. *Journal of Geophysical Research*, *116*, D15302. <https://doi.org/10.1029/2010JD015563>
- Sahu, S. K., Beig, G., & Sharma, C. (2008). Decadal growth of black carbon emissions in India. *Geophysical Research Letters*, *35*, L02807. <https://doi.org/10.1029/2007GL032333>
- Samsat, B. H., Myhre, G., Herber, A., Kondo, Y., Li, S. M., Moteki, N., et al. (2014). Modelled black carbon radiative forcing and atmospheric lifetime in AeroCom Phase II constrained by aircraft observations. *Atmospheric Chemistry Physics*, *14*(22), 12,465–12,477. <https://doi.org/10.5194/acp-14-12465-2014>
- Samsat, B. H., Myhre, G., Schulz, M., Balkanski, Y., Bauer, S., Bernsten, T. K., et al. (2013). Black carbon vertical profiles strongly affect its radiative forcing uncertainty. *Atmospheric Chemistry Physics*, *13*(5), 2423–2434. <https://doi.org/10.5194/acp-13-2423-2013>
- Shen, Z., Liu, J., Horowitz, L. W., Henze, D. K., Fan, S., Levy, H. II, et al. (2014). Analysis of transpacific transport of black carbon during HIPPO-3: Implications for black carbon aging. *Atmospheric Chemistry Physics*, *14*(12), 6315–6327. <https://doi.org/10.5194/acp-14-6315-2014>
- Stevens, R., & Dastoor, A. (2019). A review of the representation of aerosol mixing state in atmospheric models. *Atmosphere*, *10*(4), 168. <https://doi.org/10.3390/atmos10040168>
- Sun, E., Che, H., Xu, X., Wang, Z., Lu, C., Gui, K., et al. (2019). Variation in MERRA-2 aerosol optical depth over the Yangtze River Delta from 1980 to 2016. *Theoretical and Applied Climatology*, *136*(1–2), 363–375. <https://doi.org/10.1007/s00704-018-2490-9>
- Talukdar, S., Jana, S., Maitra, A., & Gogoi, M. M. (2015). Characteristics of black carbon concentration at a metropolitan city located near land-ocean boundary in Eastern India. *Atmospheric Research*, *153*, 526–534. <https://doi.org/10.1016/j.atmosres.2014.10.014>
- Tao, J., Zhang, L., Cao, J., Zhong, L., Chen, D., Yang, Y., et al. (2017). Source apportionment of PM_{2.5} at urban and suburban areas of the Pearl River Delta region, South China—with emphasis on ship emissions. *Science of the Total Environment*, *574*, 1559–1570. <https://doi.org/10.1016/j.scitotenv.2016.08.175>
- Tosca, M. G., Randerson, J. T., & Zender, C. S. (2013). Global impact of smoke aerosols from landscape fires on climate and the Hadley circulation. *Atmospheric Chemistry Physics*, *13*(10), 5227–5241. <https://doi.org/10.5194/acp-13-5227-2013>
- Twomey, S. (2007). Pollution and the planetary albedo. *Atmospheric Environment*, *41*(2007), 120–125. <https://doi.org/10.1016/j.atmosenv.2007.10.062>
- Van Der Werf, G. R., Randerson, J. T., Giglio, L., Van Leeuwen, T. T., Chen, Y., Rogers, B. M., et al. (2017). Global fire emissions estimates during 1997–2016. *Earth System Science Data*, *9*(2), 697–720. <https://doi.org/10.5194/essd-9-697-2017>
- Wang, B., & Lin, H. (2002). Rainy season of the Asian-Pacific summer monsoon. *Journal of Climate*, *15*(4), 386–398. [https://doi.org/10.1175/1520-0442\(2002\)015<0386:RSOTAP>2.0.CO;2](https://doi.org/10.1175/1520-0442(2002)015<0386:RSOTAP>2.0.CO;2)
- Wang, D., Zhu, B., Jiang, Z., Yang, X.-Q., & Zhu, T. (2016). The impact of the direct effects of sulfate and black carbon aerosols on the subseasonal march of the East Asian subtropical summer monsoon. *Journal of Geophysical Research: Atmospheres*, *121*, 2610–2625. <https://doi.org/10.1002/2015JD024574>
- Wang, H., Rasch, P. J., Easter, R. C., Singh, B., Zhang, R., Ma, P. L., et al. (2014). Using an explicit emission tagging method in global modeling of source-receptor relationships for black carbon in the Arctic: Variations, sources, and transport pathways. *Journal of Geophysical Research: Atmospheres*, *119*, 12,888–12,909. <https://doi.org/10.1002/2014JD022297>
- Wang, N., Lyu, X. P., Deng, X. J., Guo, H., Deng, T., Li, Y., et al. (2016). Assessment of regional air quality resulting from emission control in the Pearl River Delta region, southern China. *Science of the Total Environment*, *573*, 1554–1565. <https://doi.org/10.1016/j.scitotenv.2016.09.013>

- Wang, Q., Huang, R. J., Zhao, Z., Zhang, N., Wang, Y., Ni, H., et al. (2016). Size distribution and mixing state of refractory black carbon aerosol from a coastal city in South China. *Atmospheric Research*, *181*, 163–171. <https://doi.org/10.1016/j.atmosres.2016.06.022>
- Wang, R., Tao, S., Balkanski, Y., Ciais, P., Boucher, O., Liu, J., et al. (2014). Exposure to ambient black carbon derived from a unique inventory and high-resolution model. *Proceedings of the National Academy of Sciences*, *111*(7), 2459–2463. <https://doi.org/10.1073/pnas.1318763111>
- Wang, R., Tao, S., Shen, H., Huang, Y., Chen, H., Balkanski, Y., et al. (2014). Trend in global black carbon emissions from 1960 to 2007. *Environmental Science & Technology*, *48*(12), 6780–6787. <https://doi.org/10.1021/es5021422>
- Wang, R., Tao, S., Wang, W., Liu, J., Shen, H., Shen, G., et al. (2012). Black carbon emissions in China from 1949 to 2050. *Environmental Science & Technology*, *46*(14), 7595–7603. <https://doi.org/10.1021/es3003684>
- Wesely, M. L. (1989). Parameterization of surface resistances to gaseous dry deposition in regional-scale numerical models. *Atmospheric Environment*, *41*(6), 52–63. <https://doi.org/10.1016/j.atmosenv.2007.10.058>
- Wesely, M. L., & Hicks, B. B. (2000). A review of the current status of knowledge on dry deposition. *Atmospheric Environment*, *34*(12–14), 2261–2282. [https://doi.org/10.1016/s1352-2310\(99\)00467-7](https://doi.org/10.1016/s1352-2310(99)00467-7)
- Wu, D., Wu, C., Liao, B., Chen, H., Wu, M., Li, F., et al. (2013). Black carbon over the South China Sea and in various continental locations in South China. *Atmospheric Chemistry Physics*, *13*(24), 12,257–12,270. <https://doi.org/10.5194/acp-13-12257-2013>
- Wu, G. X., Li, Z. Q., Fu, C. B., Zhang, X. Y., Zhang, R. Y., Zhang, R. H., et al. (2016). Advances in studying interactions between aerosols and monsoon in China. *Science China Earth Sciences*, *59*(1), 1–16. <https://doi.org/10.1007/s11430-015-5198-z>
- Yang, Y., Liao, H., & Li, J. (2014). Impacts of the East Asian summer monsoon on interannual variations of summertime surface-layer ozone concentrations over China. *Atmospheric Chemistry Physics*, *14*(13), 6867–6879. <https://doi.org/10.5194/acp-14-6867-2014>
- Yang, Y., Wang, H., Smith, S. J., Ma, P. L., & Rasch, P. J. (2017). Source attribution of black carbon and its direct radiative forcing in China. *Atmospheric Chemistry Physics*, *17*(6), 4319–4336. <https://doi.org/10.5194/acp-2016-1032>
- Yang, Y., Wang, H., Smith, S. J., Zhang, R., Lou, S., Yu, H., et al. (2018). Source apportionments of aerosols and their direct radiative forcing and long-term trends over continental United States. *Earth's Future*, *6*, 793–808. <https://doi.org/10.1029/2018EF000859>
- Yin, X., Huang, Z., Zheng, J., Yuan, Z., Zhu, W., Huang, X., & Chen, D. (2017). Source contributions to PM_{2.5} in Guangdong province, China by numerical modeling: Results and implications. *Atmospheric Research*, *186*, 63–71. <https://doi.org/10.1016/j.atmosres.2016.11.007>
- Yu, K., Xing, Z., Huang, X., Deng, J., Andersson, A., Fang, W., et al. (2018). Characterizing and sourcing ambient PM_{2.5} over key emission regions in China III: Carbon isotope based source apportionment of black carbon. *Atmospheric Environment*, *177*, 12–17. <https://doi.org/10.1016/j.atmosenv.2018.01.009>
- Zhang, G., Li, J., Li, X. D., Xu, Y., Guo, L. L., Tang, J. H., et al. (2010). Impact of anthropogenic emissions and open biomass burning on regional carbonaceous aerosols in South China. *Environmental Pollution*, *158*(11), 3392–3400. <https://doi.org/10.1016/j.envpol.2010.07.036>
- Zhang, G. J., & McFarlane, N. A. (1995). Sensitivity of climate simulations to the parameterization of cumulus convection in the Canadian climate centre general circulation model. *Atmosphere-Ocean*, *33*(3), 407–446. <https://doi.org/10.1080/07055900.1995.9649539>
- Zhang, J., Liu, J., Tao, S., & Ban-Weiss, G. A. (2015). Long-range transport of black carbon to the Pacific Ocean and its dependence on aging timescale. *Atmospheric Chemistry Physics*, *15*(20), 11,521–11,535. <https://doi.org/10.5194/acp-15-11521-2015>
- Zhang, L., Liao, H., & Li, J. (2010). Impacts of Asian summer monsoon on seasonal and interannual variations of aerosols over eastern China. *Journal of Geophysical Research*, *115*, D00K05. <https://doi.org/10.1029/2009JD012299>
- Zhang, R., Wang, H., Hegg, D. A., Qian, Y., Doherty, S. J., Dang, C., et al. (2015). Quantifying sources of black carbon in western North America using observationally based analysis and an emission tagging technique in the Community Atmosphere Model. *Atmospheric Chemistry Physics*, *15*(22), 12,805–12,822. <https://doi.org/10.5194/acp-15-12805-2015>
- Zhang, R., Wang, H., Qian, Y., Rasch, P. J., Easter, R. C., Ma, P. L., et al. (2015). Quantifying sources, transport, deposition and radiative forcing of black carbon over the Himalayas and Tibetan Plateau. *Atmospheric Chemistry Physics*, *15*(11), 6205–6223. <https://doi.org/10.5194/acp-15-6205-2015>
- Zhang, Y. L., Li, J., Zhang, G., Zotter, P., Huang, R. J., Tang, J. H., et al. (2014). Radiocarbon-based source apportionment of carbonaceous aerosols at a regional background site on Hainan Island, South China. *Environmental Science & Technology*, *48*(5), 2651–2659. <https://doi.org/10.1021/es4050852>
- Zhao, D., Tie, X., Gao, Y., Zhang, Q., Tian, H., Bi, K., et al. (2015). In-situ aircraft measurements of the vertical distribution of black carbon in the lower troposphere of Beijing, China, in the spring and summer time. *Atmosphere*, *6*(5), 713–731. <https://doi.org/10.3390/atmos6050713>
- Zhao, P., Zhang, R. H., Liu, J. P., Zhou, X. J., & He, J. H. (2007). Onset of southwesterly wind over eastern China and associated atmospheric circulation and rainfall. *Climate Dynamics*, *28*(7–8), 797–811. <https://doi.org/10.1007/s00382-006-0212-y>
- Zhong, L., Louie, P. K., Zheng, J., Yuan, Z., Yue, D., Ho, J. W., & Lau, A. K. (2013). Science-policy interplay: Air quality management in the Pearl River Delta region and Hong Kong. *Atmospheric Environment*, *76*, 3–10. <https://doi.org/10.1016/j.atmosenv.2013.03.012>
- Zhu, C. W., Zhou, X. J., Zhao, P., Chen, L. X., & He, J. H. (2011). Onset of East Asian subtropical summer monsoon and rainy season in China. *Science China Earth Sciences*, *54*(12), 1845–1853. <https://doi.org/10.1007/s11430-011-4284-0>
- Zhu, J., Liao, H., & Li, J. (2012). Increases in aerosol concentrations over eastern China due to the decadal-scale weakening of the East Asian summer monsoon. *Geophysical Research Letters*, *39*, L09809. <https://doi.org/10.1029/2012GL051428>
- Zhu, Q. G., He, H. J., & Wang, P. X. (1986). A study of circulation differences between East-Asian and Indian summer monsoons with their interaction. *Advances in Atmospheric Sciences*, *3*(4), 466–477. <https://doi.org/10.1007/BF02657936>
- Zhuang, B. L., Chen, H. M., Li, S., Wang, T. J., Liu, J., Zhang, L. J., et al. (2019). The direct effects of black carbon aerosols from different source sectors in East Asia in summer. *Climate Dynamics*, *53*(9–10), 5293–5310. <https://doi.org/10.1007/s00382-019-04863-5>